Defence Research and   Recherche et développement
Development Canada   pour la défense Canada

DEFENCE **R&D** DÉFENSE

Analysis of high resolution polarimetry data of static targets in automatic target recognition context

Nicholas Sandirasegaram and Chen Liu

Defence R&D Canada – Ottawa
TECHNICAL MEMORANDUM
DRDC Ottawa TM 2007-330
December 2007

Canadä

Analysis of high resolution polarimetry data of static targets in automatic target recognition context

Nicholas Sandirasegaram
Chen Liu

Defence R&D Canada – Ottawa

Principal Author

Original signed by Nicholas Sandirasegaram

Nicholas Sandirasegaram

Defence Scientist

Approved by

Original signed by Gary Geling

Gary W. Geling

Head/ Radar Applications and Space Technologies Section

Approved for release by

Original signed by Pierre Lavoie

Pierre Lavoie

Chair, Document Review Panel

Abstract

Reduction of false alarm with acceptable accuracy of classification rate is a challenge in Automatic Target Recognition (ATR) using Synthetic Aperture Radar (SAR) images. This report addresses the evaluation of polarimetric techniques features, benefits of applying Two-Dimensional Fourier Transform on the polarimetric features, and the technique of training data selection to improve the classification accuracy and to reduce the false alarm in small stationary targets of high-resolution full polarimetric SAR images. The Pauli and Cameron decompositions, Self Organizing Maps, and Span techniques are applied on the polarimetric data and then Two-Dimensional Fourier Transform is applied to improve the performance. Two types of training data (one with samples of target only and the other with samples of target and Not-a-target) are used to train the Holographic Neural Technology (a neural network) classifier. The results show the Self Organizing Map feature extraction technique with Fourier Transform algorithm has a better classification rate and low false alarm. The ATR system trained with samples of target and not-a-target, produced low false alarm compared to the one trained with samples of target alone.

Résumé

Une difficulté de la reconnaissance automatique des cibles dans les images acquises par radar à synthèse d'ouverture (RSO) est bien de réduire le nombre de fausses alertes tout en conservant une précision acceptable pour la classification. Dans le présent rapport, nous nous intéressons à l'évaluation des structures décelées par les techniques polarimétriques, les avantages d'appliquer la transformée de Fourier bidimensionnelle aux structures polarimétriques et les techniques de sélection des données destinées à l'apprentissage du détecteur automatisé afin d'améliorer l'exactitude de la classification et réduire le nombre de fausses alertes pour les petites cibles stationnaires dans les images RSO à haute résolution complètement polarimétriques. Les décompositions de Pauli et Cameron, les cartes auto-organisatrices et les techniques SPAN ont été appliquées aux données polarimétriques soumises subséquemment à une transformée de Fourier bidimensionnelle afin d'améliorer le rendement. Nous avons utilisé deux ensembles de données (un ne contenant que les objets ciblés et l'autre formé d'objets ciblés et non ciblés) pour l'apprentissage du classificateur basé sur un réseau neuronal holographique (NHeT de la société AND). Nos résultats montrent que la technique d'extraction par cartes auto-organisatrices suivie d'une transformée de Fourier présente le meilleur taux de classification et le taux plus bas de fausses alertes. Le système de reconnaissance automatisée soumis à un apprentissage avec des échantillons d'objets ciblés et non ciblés a présenté moins de fausses alertes que celui formé que d'échantillons d'objets ciblés.

This page intentionally left blank.

Executive summary

Analysis of high resolution polarimetry data of static targets in automatic target recognition context

Nicholas Sandirasegaram; Chen Liu; DRDC Ottawa TM 2007-330; Defence R&D Canada – Ottawa; December 2007.

Introduction: The objective of this study is to improve the probability of target recognition and reduce the probability of false alarm using polarimetric synthetic aperture radar (PolSAR) images. Polarimetric radar adds more information by providing four linear polarization channels with both magnitude and inter-channel phase information. Polarimetric data produces more information than single polarization data, but this information is not useful unless it is properly extracted.

Well-known processing techniques including Span, Self-Organizing-Map (SOM), Pauli and Cameron decompositions are applied to extract information from the polarimetric channels and then a Fast Fourier Transform (FFT) is applied to improve the results. Holographic Neural Technology (HNeT) is then used as the classifier. The training data is divided into two sets: one with samples of four target classes and the other with samples of four target classes and three non-target classes. A high resolution X-band, spotlight mode polarimetric SAR dataset is used in this study. This data set was made available to the members of the NATO (Sensors & Electronics Technology panel) SET-053 task group by QinetiQ Ltd.

Results: Many Automatic Target Recognition (ATR) systems were analyzed based on measures of performance such as percentage of correct classification over detected targets and percentage of false alarms. Analysis is conducted on effects of selection of the training dataset, the usage of the FFT technique, the Cameron decomposition method on segmented and non-segmented targets, and a comparison of ATR systems based on full and single channel datasets.

The results show that using polarimetric data in a neural network based SOM followed by the application of the FFT has the highest number of correct classifications and the lowest number of false alarms compared to the other techniques that are investigated in this report. The classifiers presented fewer false alarms when they were trained using a dataset that contained samples for both the training target and the non-target dataset.

Significance: This study will help in selection of appropriate methods for implementations in future ATR systems. In addition, it will assist Image Analysts (IAs) to choose the appropriate techniques and selection of training datasets to perform their tasks.

Sommaire

Analysis of high resolution polarimetry data of static targets in automatic target recognition context

Nicholas Sandirasegaram; Chen Liu; DRDC Ottawa TM 2007-330; R & D pour la défense Canada – Ottawa, December 2007.

Introduction : Cette étude avait comme objectif (1) d'accroître la probabilité de reconnaissance des cibles et (2) de réduire celle des fausses alertes dans les images obtenues par radar à synthèse d'ouverture polarimétrique. Le radar polarimétrique donne de renseignements, ils sont renfermés dans les quatre canaux de polarisation linéaire et les données sur l'intensité et les différences de phase entre les canaux. Or, bien que les données polarimétriques contiennent plus d'informations que les données monopolarisées, elles ne seront pas utiles si l'on ne parvient pas à les extraire correctement.

Pour extraire des informations des canaux polarimétriques, nous avons d'abord appliqué des techniques de traitement bien connues — technique Span, cartes auto-organisatrices, décompositions de Pauli et Cameron — puis nous les avons soumis à une transformée rapide de Fourier (FFT) pour améliorer la qualité des résultats que nous avons classifiés en utilisant la technologie HNeT (réseaux neuronaux holographiques). Le classificateur a subi un apprentissage basé sur deux ensembles de données : un premier constitué de quatre classes de cibles et un second formé d'échantillons de quatre classes d'objets ciblés et de trois classes de d'objets non ciblés. Les données provenaient d'un ensemble de données RSO polarimétriques, à haute résolution, dans la bande X obtenues en mode « spotlight », offertes par QuinetiQ Ltd, aux membres du groupe de travail SET-053 (comité de la technologie des capteurs et de l'électronique).

Résultats : Plusieurs systèmes de reconnaissance automatique des cibles ont été analysés à l'aide de mesures de rendement comme le pourcentage de cibles correctement classées, par rapport au nombre de cibles détectées ou, encore, le pourcentage de fausses alertes. Nous avons analysé les effets du choix de l'ensemble de données servant à l'apprentissage, de l'utilisation de la transformée de Fourier, de la méthode de décomposition de Cameron sur les cibles segmentées et non segmentées. Nous avons également comparé les résultats des systèmes de reconnaissance automatique des cibles exploités sur des ensembles de données complètement polarimétriques ou monocanal.

Nos résultats montrent que, de toutes les techniques étudiées, c'est le traitement des données polarimétriques dans une carte auto-organisatrice basée sur un réseau neuronal, suivi par l'application d'une FFT qui produit le nombre le plus élevé de classifications correctes et le nombre le plus bas de fausses alertes. Les classificateurs qui ont donné le moins de fausses alertes sont ceux où l'on avait dont l'apprentissage avait été réalisé à l'aide d'ensembles contenant des objets ciblés et non ciblés.

Importance : Cette étude contribuera aux choix des méthodes qui seront imbriquées dans les futurs systèmes de reconnaissance automatique des cibles. En outre, elle facilitera la tâche des

analystes d'image lorsqu'ils détermineront quels techniques et ensembles d'apprentissage sont les plus appropriés.

This page intentionally left blank.

Table of contents

List of figures

List of tables

Acknowledgements

This page intentionally left blank.

1   Introduction

Nowadays, many radar sensors [[1], [2]] are collecting large amount of radar images of target of interest and there is neither time nor enough manpower (Image Analysts) to go through each scene of the collected data. There is a need for automated methods to extract targets of interest from the larger scene. So far, many researchers have developed automated algorithms and tools [[3]-[6]], but there is still a need for more improvement in the recognition rate and the false alarm reduction.   This study is conducted to contribute a value to improve correct recognition rate and to reduce false alarm using automated algorithms. This will assist Image Analysts in performing their tasks.

Polarimetric spot Synthetic Aperture Radar (SAR) data is used for this study. Full polarimetric data have more information than single polarization data but those information aren't useful if they are not extracted properly from the full polarimetric data. A number of techniques were applied on the polarimetric images and classification results were analyzed.

Span, Self-Organizing-Map (SOM), Pauli and Cameron decompositions are applied to extract useful information from the polarimetric channels and then Fast Fourier Transform (FFT) is applied to improve the results. Holographic Neural Technology (HNeT) is used as a classifier in this analysis. Training data is divided into two sets; one with samples of four target classes and the other with samples of four target classes and three not-a-target classes. These methods are described in the coming sections.

2   Polarimetry data of static targets

The data used in this investigation are collected as high resolution spotlight polarimetric SAR images in the X-band. The data are composed of four classes of targets and 5 classes of non-targets. QinetiQ made these data available to members of the NATO SET-053 task group. The name of the targets and non-targets are not given to the group.

Target classes are named A, B, D and G and non-target classes are named C, E, F, H and I. Here, "target" and non-targets mean target of interest and not target of interest respectively. We separated non-target classes into two groups; one group called not-a-target and the other group called confuser. The non-target classes C, E, and F are assigned to not-a-target group and the H & I are assigned to confuser group. The target and not-a-target group classes are formed into two sets of training datasets.   One of the training dataset contains samples of target classes only (Table 1) and the other one contains samples of target and not-a-target group classes (Table 2). Only one testing dataset was formed from the target and confuser group classes (Table 3), which is different from the training datasets. That is, the samples of testing dataset are not included in the training dataset.

Table 1. Training dataset – samples of target

Target type		# of samples
Targets	A	330
	B	335
	D	335
	G	335

Table 2. Training dataset – samples of target and not-a-target

Target type		# of samples
Targets	A	330
	B	335
	D	335
	G	335
Not-a-target	C	335
	E	335
	F	335

Table 3. Testing dataset – samples of target and confuser

Target type		# of samples
Targets	A	110
	B	110
	D	110
	G	110
Confusers	H	110
	I	110

3   Preprocessing Methods

Standard preprocessing methods applied to the images are described below. These methods
are called rotation, segmentation, centering and cropping.   One or more of these
preprocessing methods are used in the ATR processing as described in section 6.0.

3.1   Rotation

The orientation of target varies in each chip and the angle of target orientation is given in the
header file. All the images are rotated to vertical orientation.

3.2   Segmentation

Median filter is applied to reduce noise in the image and then a threshold value is applied to
remove the pixel that has less reflectivity for the radar signal. The threshold is the median
value of the filtered image. Then blocks are formed from the selected pixels. The largest
block is separated from the background as this block contains the target information.

3.3   Centering

Two different methods can be used to find the center of the chip. One method uses highest
reflectivity point on the target as the centre point. This method applies median filter to reduce
the noise and then finds the highest reflectivity point on the filtered image. The other one uses
center mass to locate the center point. This method is applied after segmenting the target.

3.4   Cropping

After locating the center, each image is cropped in with this center point as its center and the
size of the cropped image is 64 by 64 pixels. This size is adequate for our application and this
chip has minimum background information.

4 Polarimetric and Feature extraction Techniques

Feature extraction is an important step in achieving good performance of ATR systems. However, the other steps in the ATR scheme also need to be optimized to obtain the best possible performance. Extraction of certain attributes of each target image is needed by classifiers to differentiate target classes.

The data focussed on this report is fully Polarimetric data, which contains four channels; Horizontal transmit and receive (HH), Horizontal transmit and Vertical receive (HV), Vertical transmit and receive (VV), and Vertical transmit and Horizontal receive (VH) polarizations. So, the feature extraction algorithms should use these four channels in extracting features to improve the separation between target types. Four feature extraction algorithms were applied in this report and they are Span, SOM, Pauli and Camereon decomposition.

4.1 Span

The classifier uses Span of the image to recognize different classes of land targets in this study.   For polarized images, the Span measure adopted is the sum of the three polarization channels. Mathematical representation [[7]] of the Span is described below

$$\text{Span} = |HH|^2 + 2\,|HV|^2 + |VV|^2. \tag{1}$$

HV = VH (under reciprocity assumption) is assumed in the Span calculations.

4.2 Self Organizing Map (SOM)

T. Kohonen has described the Self-Organizing Map (SOM) in the early 1980s [[8]]. The SOM is a feed forward Neural Network with single layer network as shown in the [[8]]. Three input and twenty five output nodes are selected for this application.   It is trained using unsupervised training method with samples of data.

Initial weights are selected from a uniform distribution on the interval between 0.0 and 1.0. All twenty-five outputs (distance) are calculated using these weights and an input vector for every iteration. The sum of the one dimensional Euclidean distances is shown in the equation below.

$$O_j = \sum_{i=1}^{N} \left| I_i^s - W_{ij} \right|, \text{ N=3, i=1,2,3, and j=1,2,3…25.} \tag{2}$$

Where O_j is the output, I_i^s is the sth input data and W_{ij} are the weights.   Each output node is computed using the above equation and the first three minimum error nodes are selected for a weights update. Weights are updated using the following equation [[9]]

$$W_{ij}(t+1) = W_{ij}(t) + LR * NF * \left(I_i^s - W_{ij}(t)\right) \qquad (3)$$

LR is the learning rate constant (0.1 in this study), t is the current iteration, and the NF is neighbourhood function, value of which is 1.0 for the first lowest error node, 0.1 for the next lowest error node and 0.01 for the third minimum error node. Three lowest error node's weights are updated in each iteration. This weights update process continues with all the input data and then repeats again five times (five epochs) for all of the input data.
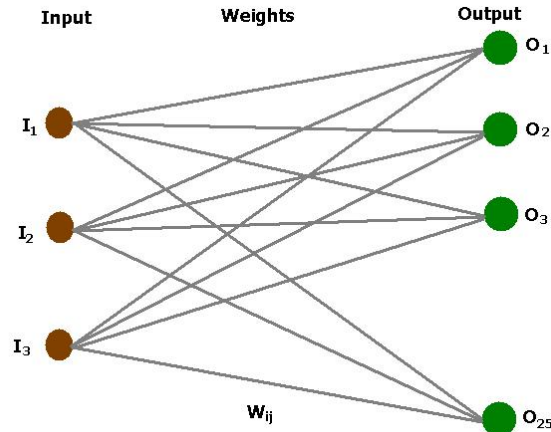
Figure 1: Three inputs and twenty-five outputs SOM.

After training the SOM, the minimum distance node for each input data is generated and then statistical information about each node is computed (see an example in Figure 2a). Here, the computed statistic is the number of times each output node is selected using the training data. The node that was selected by maximum number of inputs is ranked 1, the node that was selected by second maximum number of inputs is ranked 2 and so on. If more than one node is selected by the same number of inputs, then those nodes are randomly selected in an order and ranked.

Based on these rank values, a constant value is assigned to these output nodes. The constant values for each node is calculated as shown below (see an example in Figure 2b)

$$NCV_i = 1 - (1/N) * Rank, \quad N=25, Rank = 1 \text{ or } 2 \text{ or } 3 \dots \text{ or } 25, i=1,2,3\dots25. \qquad (4)$$

where NCV_i is the node constant value for node i. There are three inputs to the SOM and these inputs are pixels, which come from three different polarizations (HH, HV and VV) or polarization combinations (HH+VV, HH–VV, HV–VH). Therefore, each pixel from three polarization (or polarization combinations) is converted to a NCV value (see Figure 3).
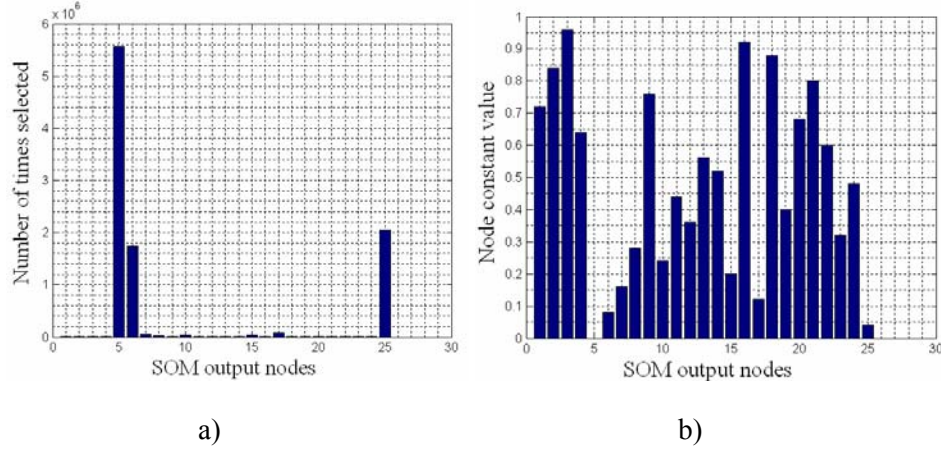
Figure 2: SOM's 25 output nodes; a) Number of times selected training data and b) Node constant value for each output node.
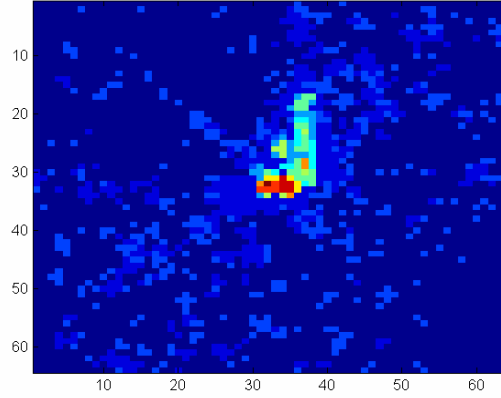
Figure 3: Example of a target image converted to node constant values.

4.3   Pauli Decomposition

Polarimetric synthetic aperture radar (PolSAR) systems provide the polarimetric signature of a target, consisting of the four elements of the scattering matrix, each containing amplitude and phase information related to the polarimetric scattering processes   A linear polarization scattering matrix **S** can be expressed in the Pauli basis [10],

$$\Psi_p = \left\{ \sqrt{2} \begin{bmatrix} 1 & 0 \\ 0 & 1 \end{bmatrix} \quad \sqrt{2} \begin{bmatrix} 1 & 0 \\ 0 & -1 \end{bmatrix} \quad \sqrt{2} \begin{bmatrix} 0 & 1 \\ 1 & 0 \end{bmatrix} \quad \sqrt{2} \begin{bmatrix} 0 & -i \\ i & 0 \end{bmatrix} \right\} \tag{5}$$

It permits the extraction of physical information from the 2×2 coherent scattering matrix. Under reciprocity assumption, (i.e., $S_{HV} \cong S_{VH}$), the Pauli scattering vector is given by [10]

$$k = \tfrac{1}{\sqrt{2}}[S_{HH} + S_{VV} \quad S_{HH} - S_{VV} \quad S_{HV} + S_{VH}]^T \tag{6}$$

The $(S_{HH} + S_{VV})$ component would tend to be large for single bounce scattering, while $(S_{HH} - S_{VV})$ would be large for double bounce, and $(S_{HV} + S_{VH})$ presents volume scattering.

In this experiment, we used the following scattering mechanisms to extract meaningful information from the polarimetric data.

$$|HH + VV| = |S_{HH} + S_{VV}|$$

$$|HH - VV| = |S_{HH} - S_{VV}| \tag{7}$$

$$|HV + VH| = |S_{HV} + S_{VH}|$$

The physical interpretation of the three basic scattering mechanisms is illustrated in Figure 4 [11].
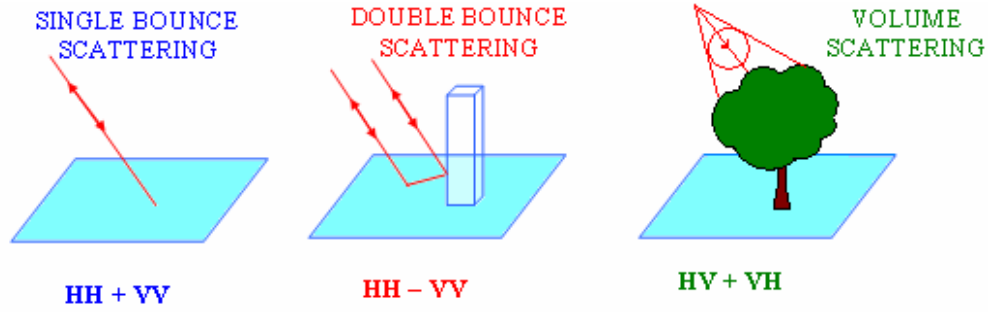
Figure 4. Physical interpretation of three basic scattering mechanisms

4.4　Cameron decomposition method

In the Cameron method, the measured scattering matrix is decomposed based on two basic properties of radar returns: reciprocity and symmetry. An arbitrary scattering matrix could be coherently decomposed into a nonreciprocal component, a maximum symmetric component and minimum symmetric component. In this report, only maximum symmetric scattering components are studied. These components are trihedral, diplane (dihedral), dipole, cylinder, narrow diplane and quarter wave device [12]. The symmetric scatterers are represented on a Unit disk as shown in Figure 5 [[12], [13]].
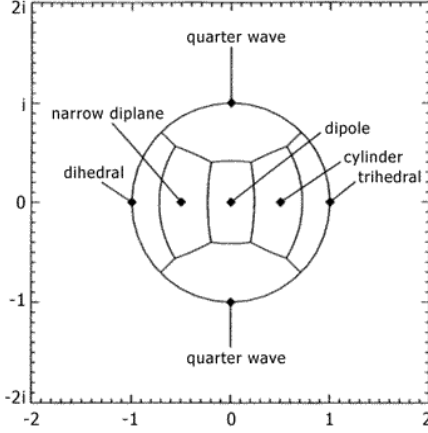
Figure 5: Cameron's Unit disc representation

A symmetric scatter can be represented in terns of the its normalized diagonal scattering matrix $\Lambda(z)$:

$$\Lambda(z) = \frac{1}{\sqrt{1+|z|^2}} \begin{pmatrix} 1 \\ 0 \\ 0 \\ z \end{pmatrix} \qquad \text{Where } z = \pm 1, \pm 0, \pm\frac{1}{2} \text{ and } \pm I \qquad (8)$$

The six elemental scatters expressed in terms of $\Lambda(z)$ as below:

Table 4. Six elemental scatters expressed in terms of z

Trihedral	diplane/di hedral	dipole	cylinder	narrow diplane	¼ wave
$\Lambda(1)$	$\Lambda(-1)$	$\Lambda(0)$	$\Lambda(\frac{1}{2})$	$\Lambda(-\frac{1}{2})$	$\Lambda(\pm i)$

Each pixel is then assigned to one of the six classes, depending on which of the components is the shortest distance according to the symmetric scatter distance measure *d*:

$$d(z_1, z_2) = \cos^{-1}\left[\frac{\max(|1 + z_1 z_2^*|, |z_1 + z_2^*|)}{\sqrt{1+|z_1|^2}\sqrt{1+|z_2|^2}} \right], \qquad 0 \le d \le \frac{2}{\pi} \qquad (9)$$

In general, trihedral represents odd bounce scattering while diplane represents even bounce scattering as in Pauli decomposition. Cylinder represents curved metallic plates, large diameter or pipe-like objects.

The following three representations are used in our experiment;

1. Cameron's unit disc representation,
2. Six elemental classes of scatterers and one non-class of scatterers and
3. Histogram from the above seven classes

In this experiment the Cameron's unit disc is quantized into 64 equal steps from –1 to +1 in real and imaginary axes. Then a two-dimensional histogram is formed using the complex Cameron's unit disc representation value (see Figure 6a). We call this feature " Unit disc representation" in this report. Another histogram feature is formed using the six elemental classes and non-class scatters. Then the histogram is normalized by total number of pixels (see Figure 6b). This feature is called "Histogram classification" feature. Third feature is replacing each pixel location by one of the seven classes of scatters (see Figure 6c) and the feature is called "Pixel classification".

a) Unit disc representation   b) Histogram classification   c) pixel based classification
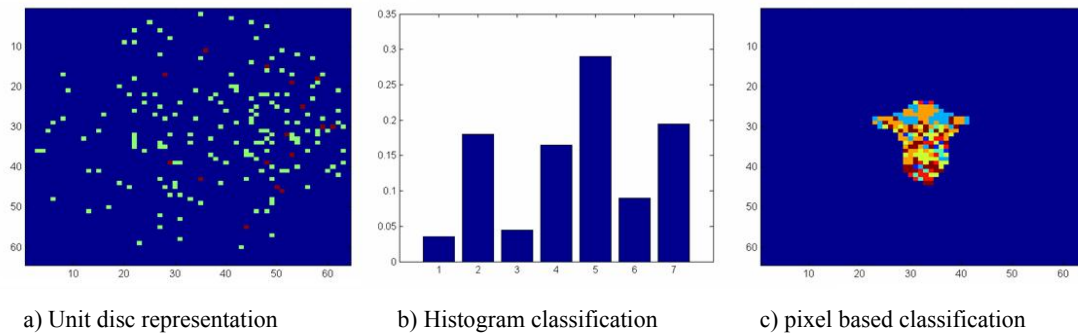
Figure 6. Examples to Cameron's decomposition method

4.5 Two-Dimensional Fast Fourier Transform (2DFFT) Technique

The two-dimensional fast Fourier transform (2DFFT) technique is applied to extract frequency contents from the 2D data formed by polarimetric or preprocessed techniques.   The 2DFFT [[15], [16]] and the properties of 2DFFT are described in [[17]]. AND Corporation has developed a tool for building applications with Holographic/Quantum Neural Technology (HNeT). The 2DFFT algorithm is built-in in this commercial software and the output of this algorithm transferred to the classifier internally. The HNeT classifier can take external input from any other external algorithms instead of using the 2DFFT algorithm or any other internal algorithms. This means, any ATR system can use HNeT classifier with any other external feature extraction algorithms.

5 Classifier

The purpose of a classifier is to identify known targets based on the information that is available to the classifier. This can be done by using either a learning method or storing target features from target of interest in a library for comparison. The classifier that we are using here is the Holographic Neural Technologies (HNeT) classifier. It is commercial software and is based on artificial neural network technology. HNeT uses the supervised learning method to train the classifier. Technical information about the HNeT classifier can be found in the references [[18] - [23]].

6   Applied ATR methods

In this report, Span, Pauli, SOM, and Cameron techniques are applied on the polarimetric images to extract useful information for classification. These methods are used in a different parts of the ATR processing chain. Span and Pauli techniques are used at the beginning of the chain. The SOM and Cameron techniques are used in the middle of the chain.

6.1   Span and Pauli based ATR methods

Span and Pauli techniques are applied directly on the image and then preprocessing methods are applied to the data. The preprocessing methods used are rotation, centering and cropping. Figure 7 shows the ATR process using Span and Pauli feature extraction methods.
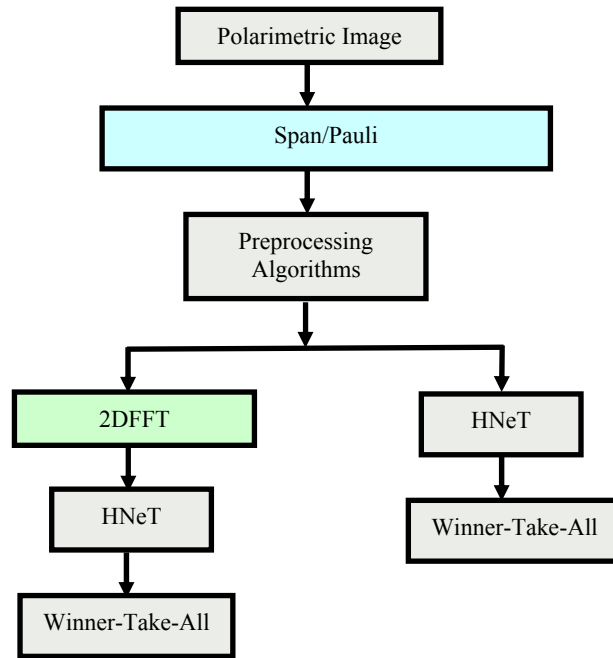
Figure 7. Span, Pauli, and single channel features based ATR methods

After preprocessing, two different approaches are followed. One of the approaches is to apply the HNeT classifier to the pre-processed data.   The second approach is to apply the 2DFFT before the HNeT classifier is applied. Thus, two classification results are obtained for each image per technique (Span and Pauli).

6.2 Self Organizing Map based ATR method

Figure 8 shows the ATR processing using the SOM. First, selected polarimetric techniques are applied to the Polarimetric image. The selected technique is Pauli method or absolute values of single channels (|HH|, |HV| and |VV|). Then preprocessing methods; rotation, centering and cropping are applied to the data. After the SOM is applied on the preprocessed data, the ATR process follows two different paths (see Figure 8). In one of the paths, SOM output is directly fed into the HNeT classifier. In the other path, 2DFFT is applied before being fed into the HNeT classifier. In this SOM approach, two separate classification results are obtained for each polarimetric image.

```
        ┌──────────────────────┐
        │  Polarimetric Image  │
        └──────────┬───────────┘
                   │
        ┌──────────▼───────────────┐
        │ |HH|, |HV| and |VV| / Pauli │
        └──────────┬───────────────┘
                   │
        ┌──────────▼───────────────┐
        │  Preprocessing Algorithms │
        └──────────┬───────────────┘
                   │
             ┌─────▼─────┐
             │    SOM    │
             └─────┬─────┘
          ┌────────┴────────┐
          │                 │
          │          ┌──────▼──────┐
          │          │    2DFFT    │
          │          └──────┬──────┘
     ┌────▼────┐       ┌─────▼─────┐
     │  HNeT   │       │   HNeT    │
     └────┬────┘       └─────┬─────┘
┌─────────▼────────┐ ┌───────▼──────────┐
│ Winner-Take-All  │ │ Winner-Take-All  │
└──────────────────┘ └──────────────────┘
```
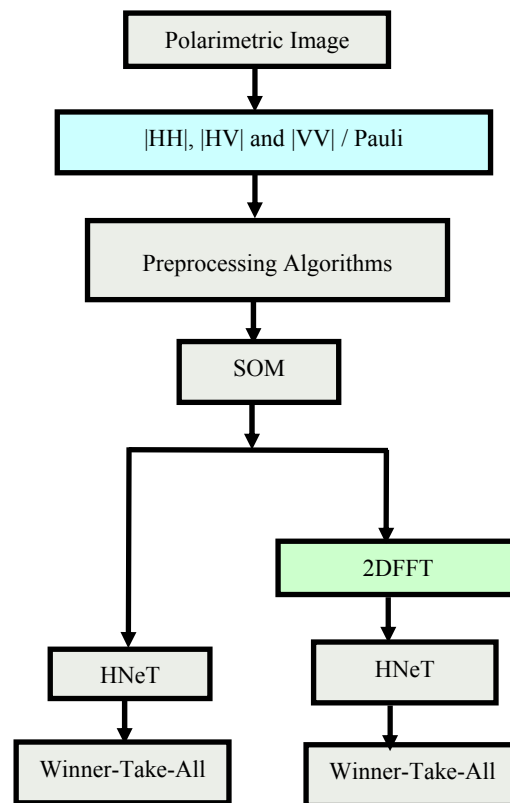
Figure 8. SOM based ATR method

6.3 Cameron decompositions based ATR method

In this report, the Cameron decomposition method is applied on both segmented and non-segmented polarimetric images. In the first step the polarimetric image with or without segmentation is centered and cropped. In this process (segmentation, centering, or cropping), the pixel values (real and imaginary) of the target are not altered, but the background/clutters

are removed during segmentation. The Cameron decomposition method is applied to the cropped chip. The Cameron decomposition is represented in three different forms; Unit Disk, Histogram, and Pixel classification. These representations are processed separately to classify the polarimetric image. The three representations are classified in two different ways as shown in the Figure 9. In one case the features are directly applied to the HNeT classifier. For the other case the features are fed into a 2DFFT before being fed into the HNeT classifier. By this method two classification results are obtained for each feature and therefore a total of six classification results are obtained for each polarimetric image.
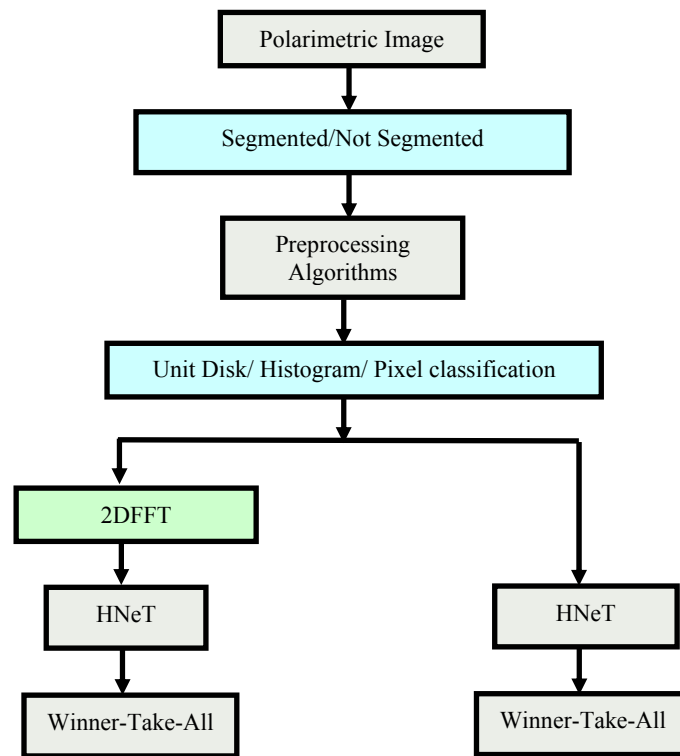
Figure 9. Cameron decompositions based ATR method

7   Experimentation Results and Analysis

The purpose of this experiment was to measure the effects of various polarimetric techniques and training methods on the false alarm and correct recognition rate. Receiver Operating Characteristic (ROC) curves and confusion matrix techniques are used for measuring the effects on the correct recognition rate and false alarm [[24] - [26]]. In the ROC curve, the X axis shows the percentage of false alarm (P_{fa}) and the Y axis shows the percentage of detection (P_d). Each point (P_{fa},P_d) on the ROC curve is calculated using various threshold values at the output of the classifier. The formulas for P_{fa} and P_d are given below.

$$P_{fa} = \frac{\text{Number of confusers detected as a target class}}{\text{Total number of confusers}} \tag{10}$$

$$P_d = \frac{\text{Number of targets detected as one of the target classes}}{\text{Total number of targets}} \tag{11}$$

Typically, the evaluation experiment is done with Pd set to 0.9.   Therefore, a confusion matrix is generated at a specific threshold setting to produce 90% of targets and to reject the rest. All the ROC curves and confusion matrices of individual tests are detailed in the Annex A. We calculated average percentage of correct classification over detected targets ($\overline{P_{cc/d}}$) for each confusion matrix as given below.

$$\overline{P_{cc/d}} = \frac{\sum\limits_{i=1}^{N} NC^i}{\sum\limits_{i=1}^{N} TD^i} , \tag{12}$$

where NC^i is number of targets correctly classified in target class i, TD^i is total number of detected targets for the target class i, and N is the total number target classes. This section shows only the $\overline{P_{cc/d}}$ and P_{fa} of the individual test results instead of showing the entire test results in detail.

The Pauli, SOM, Span, Cameron decomposition, and single channel techniques are analyzed and the results are reported in this section. The Pauli technique extracted four sets of different representations. These sets are |HH–VV|, |HH+VV|, |HV+VH| and the Pauli-three (|HH–VV|, |HH+VV| and |HV+VH| combined to form one set). The SOM uses two different forms of input, one is a single channel combination of |HH|, |HV| and |VV| and the other one is a Pauli combination of |HH–VV|, |HH+VV| and |HV+VH|. Three different representations are formed from Cameron decomposition features and they are pixel classification representation, unit disc representation and histogram classification representation. The single channel technique uses the co-polarization channels (|HH| and |VV|). In this analysis, these polarimetric and single channel techniques are tested and the results are listed separately in the tables.

Training and testing datasets, used in this experiment are described in section 2. These datasets are formed from the four target types (A, B, D, and G), 2 confuser types (H and I) and 3 not-a-target types (C, E, and F).

Analysis is conducted in many aspects including selection of training data, effect of using the 2DFFT technique on the extracted features, and benefits of using of segmented targets. In addition, polarimetric and single channels based ATR systems are compared with each other. The following topics are explored further in the following sections;

- Selection of training dataset

- 2DFFT technique

- Cameron method on segmented and not segmented targets

- Comparison of ATR systems based on full and single channels datasets

7.1 Selection of training dataset

Two training datasets are formed (see section 2.0). The difference between these two datasets is that one set contains only samples of target types while the other training dataset includes samples of target types as well as samples of not-a-target type. Thus, a total of two separate training datasets and one testing dataset are selected for this experiment. All the different ATR methods are trained with these two datasets separately and then tested on the same testing dataset. Each of the ATR system was trained to recognize all of the four targets. Experiments are conducted with both the training datasets using Span, Pauli and SOM methods. The results were generated in the form of confusion matrices (Table A.1, Table A.2, Table A.3 and Table A.5) at P_d equal to 90% and ROC curves (Figure A.1, Figure A.2, Figure A.3 and Figure A.5), and they are listed in the Annex A.

The ATR systems with and without normalized preprocessed data and 2DFFT approaches are used (see section 6.0 for more details of the ATR process) in this experiment to produce Table 5. Table 5 shows the $\overline{P_{cc/d}}$ of each ATR process. The $\overline{P_{cc/d}}$ result with the 2DFFT technique shows slightly better results when the classifiers are trained with the dataset which contains only samples of target types. However, the ATR process using all the Pauli features shows better $\overline{P_{cc/d}}$ rate with the training dataset which contains target and not-a-target samples. All classifiers (except the classifier which uses all of the Pauli features) using normalization and 2DFFT technique trained with target and not-a-target samples performed well in $\overline{P_{cc/d}}$ compared to the classifiers trained with the target samples only. However, for the ATR process using all of the Pauli features, the classifier trained with only the target samples performed slightly better than the classifier trained with the target and not-a-target samples. The above examples of $\overline{P_{cc/d}}$ performance indicate that all of the classifiers trained with both

types of training datasets give similar performance.

Table 5. Summary of $\overline{P_{cc/d}}$ using the both training datasets at $P_d = 90\%$.

Features		2DFFT		Normalized & 2DFFT	
		Trained using samples of		Trained using samples of	
		target	target & not-A-target	target	target & not-A-target
Pauli	|HH+VV|	73.48	62.22	91.16	92.42
	|HH-VV|	73.87	67.93	92.44	93.43
	|HV+VH|	83.84	82.58	92.68	95.20
	Pauli-three	88.38	91.41	96.97	95.96
SOM	HH_HV_VV	94.95	92.42	98.23	98.99
	Pauli	95.45	93.94	97.98	97.98
Span		56.78	51.01	90.91	91.41

Table 6. Summary of average false alarm using the both training datasets at $P_d = 90\%$.

Features		2DFFT		Normalized & 2DFFT	
		Trained using samples of		Trained using samples of	
		target	target & not-A-target	target	target & not-A-target
Pauli	|HH+VV|	66.82	30.45	60.45	35.00
	|HH-VV|	91.82	49.09	74.55	36.36
	|HV+VH|	97.73	30.45	82.27	13.18
	Pauli-three	95.45	22.73	60.45	17.27
SOM	HH_HV_VV	81.36	32.27	37.73	8.18
	Pauli	88.64	25.91	51.36	17.27
Span		100.00	93.18	81.36	64.55

Experimentation results of P_{fa} study using these two training datasets are shown in Tables A.1.1, A.1.2, A.2.1 and A.2.2 (Annex A). Those results are averaged and summarized here in Tables 5 and 6. P_{fa} is much lower when trained with the dataset that has both target and not-a-target samples than when trained with the datasets that have only target type samples. Overall, the classifiers trained on the target and not-a-target samples have a better P_{fa} and almost the same $\overline{P_{cc/d}}$ performance.

7.2   2DFFT technique

Here, 2DFFT technique is investigated to see its effect on the correct classification rate and false alarm. To achieve this ATR system is implemented with and without 2DFFT technique in the process. The tested ATR systems are formed with various features, and with and without 2DFFT techniques. Both the training datasets are used in this experiment.

The results are shown in Annex A. *Table 7* shows the summary of $\overline{P_{cc/d}}$ for SOM, Span and Pauli based feature methods. The results show that all of the ATR systems performed well when the 2DFFT technique is applied to the dataset. Table 8 shows the summary of the $\overline{P_{cc/d}}$ for the decomposition methods. The 2DFFT technique worked well for the pixel classification and unit disk representation methods but not for the histogram classification method. The histogram classification method used one dimensional features and a total of 7 features for each target. This low number of features is not sufficient enough to produce accurate frequency information for use by the 2DFFT technique.

Table 7. Summary of $\overline{P_{cc/d}}$ using the both with and without 2DFFT techniques at $P_d = 90\%$.

Features		Trained using target & not-A-target samples	
		Without 2DFFT	*With 2DFFT*
P a ul i	*|HH+VV|*	77.02	92.42
	|HH-VV|	79.15	93.43
	|HV+VH|	73.48	95.20
	Pauli-three	86.62	95.96
S O M	*HH_HV_VV*	66.67	98.99
	Pauli	77.27	97.98
Span		83.63	91.41

Table 8. Summary of $\overline{P_{cc/d}}$ using Cameron decomposition method, and the both with and without 2DFFT techniques at P_d = 90%.

Features	Trained using target & not-A-target samples			
	Not-Segmented		Segmented	
	Without 2DFFT	With 2DFFT	Without 2DFFT	With 2DFFT
Pixel classification	32.39	43.99	64.62	85.60
Unit Disc Representation	26.41	37.34	24.68	27.76
Histogram classification	42.67	23.23	25.19	24.68

The percentages of false alarm are calculated and the results are listed in Annex A. These results are summarized in Table 9 and Table 10. Table 9 shows the average P_{fa} of the SOM, Pauli and Span feature based ATR systems. The P_{fa} is reduced in all the feature based ATR systems. Applying the 2DFFT technique to the Cameron pixel classification datasets (with and without segmented targets), reduces the false alarm. This is also true for the unit disc representation of segmented targets. However, the 2DFFT technique could not reduce the false alarm in the histogram classification feature based ATR system or the unit disc representation non-segmented feature based ATR system.

Table 9. Summary of P_{fa} using the both with and without 2DFFT techniques at P_d = 90%.

Features		Trained using target & not-A-target samples	
		Without 2DFFT	With 2DFFT
P a ul i	**|HH+VV|**	76.82	35.00
	|HH-VV|	80.45	36.36
	|HV+VH|	73.18	13.18
	Pauli-three	66.36	17.27
S O M	**HH_HV_VV**	47.27	8.18
	Pauli	65.45	17.27
Span		83.18	64.55

Table 10. Summary of P_{fa} using Cameron decomposition method, and the both with and without 2DFFT techniques at $P_d = 90\%$.

Features	Trained using target & not-A-target samples			
	Not-Segmented		Segmented	
	Without 2DFFT	With 2DFFT	Without 2DFFT	With 2DFFT
Pixel classification	83.80	77.31	74.54	29.63
Unit Disc Representation	86.11	87.96	75.93	63.43
Histogram classification	70.37	91.20	47.22	87.96

As seen from the tables, the $\overline{P_{cc/d}}$ for Span and |HH+VV| feature based ATR systems is less than that of other ATR systems and the percentage of false alarm for Span based ATR system is higher than that of the other systems. The above is true for the decomposition method of histogram and unit disc representation based ATR systems. That is, the 2DFFT technique is unable to extract useful frequency information from these features compared to other types of features.

7.3   Cameron decomposition method on segmented and non-segmented targets

The Cameron method was applied on segmented and non-segmented targets. Extracted features are represented by three forms of feature sets, pixel classification, unit disc representation, and histogram classification. Then these features are fed into the HNeT classifier to recognize the target. Two approaches have been taken in feeding the features into the HNeT classifier. In one approach, features are fed directly into the HNeT classifier. In the other approach, a 2DFFT is applied before being fed into the HNeT classifier. Experimental results are listed in the Annex A for each target type. Here, the summary of average $P_{cc/d}$ and P_{fa} are listed in *Table 11* and *Table 12* respectively. The unit disc representation and histogram classification approaches performed well with non-segmented targets. However, the $P_{cc/d}$ is less than 50%. In the Pixel classification approach, however, the $\overline{P_{cc/d}}$ is more than 60% on the segmented targets and less than 45% on the not segmented targets. The highest $\overline{P_{cc/d}}$ of 85.6% is achieved on the segmented target using pixel classification features. P_{fa} is lower on the segmented targets than on non-segmented targets in all the features. The lowest P_{fa} is achieved (29.6%) with the segmented target using pixel classification features.

Table 11. Summary of $\overline{P_{cc/d}}$ using Cameron method with and without segmentation technique at $P_d = 90\%$.

Features	Trained using target & not-A-target samples			
	No additional techniques		*2DFFT*	
	Not Segmentation	*Segmentation*	*Not Segmentation*	*Segmentation*
Pixel classification	32.39	64.62	43.99	85.60
Unit Disc Representation	26.41	24.68	37.34	27.76
Histogram classification	42.67	25.19	23.23	24.68

Table 12. Summary of $\overline{P_{cc/d}}$ using Cameron method with and without segmentation technique at $P_d = 90\%$.

Features	Trained using target & not-A-target samples			
	No additional techniques		*2DFFT*	
	Not Segmentation	*Segmentation*	*Not Segmentation*	*Segmentation*
Pixel classification	83.80	74.54	77.31	29.63
Unit Disc Representation	86.11	75.93	87.96	63.43
Histogram classification	70.37	47.22	91.20	87.96

7.4 Comparison of ATR systems

A good ATR system provides fewer false alarms while providing high correct identification rate. Therefore, P_{fa} and $\overline{P_{cc/d}}$ are used as parameters to compare the ATR system. At $P_d = 90\%$, the values of P_{fa} and $\overline{P_{cc/d}}$ are obtained and using the equation, $M = (\overline{P_{cc/d}} - P_{fa})$, the value of "M" is calculated. The ATR system which provides the highest value of "M" is the best ATR system.

Table 13. Summary of the ATR metric 'M' value for each feature based ATR system
at P_d = 90%.

Features		Trained using target & not-A-target samples	
		$(\overline{P_{cc/d}} - P_{fa})$	*Additional Technique*
P a ul i	*|HH+VV|*	57.42	2DFFT
	|HH-VV|	57.07	2DFFT
	|HV+VH|	82.02	2DFFT
	Pauli-three	78.69	2DFFT
S O M	*HH_HV_VV*	90.81	2DFFT
	Pauli	80.71	2DFFT
Span		29.76	No additional Technique
Pixel classification		55.97	2DFFT and Segmented targets
Unit Disc Representation		-35.66	2DFFT and Segmented targets
Histogram classification		-22.03	Segmented targets

Table 13 gives the summary of the 'M' value for each feature based ATR. Figure 10 shows the bar plot of the percentage difference between best $\overline{P_{cc/d}}$ and P_{fa} for each ATR system. The bar plot shows the same information as in the Table 13 but it is presented in a form that makes comparison much easier. SOM with HH_HV_VV features performed well compared to other systems. However, the performance of the Pauli-three, |HV + VH|, and SOM with Pauli methods are also relatively similar. Most of the ATR systems performed well when the both feature enhancement methods (Normalized and 2DDFT) were applied to the features.
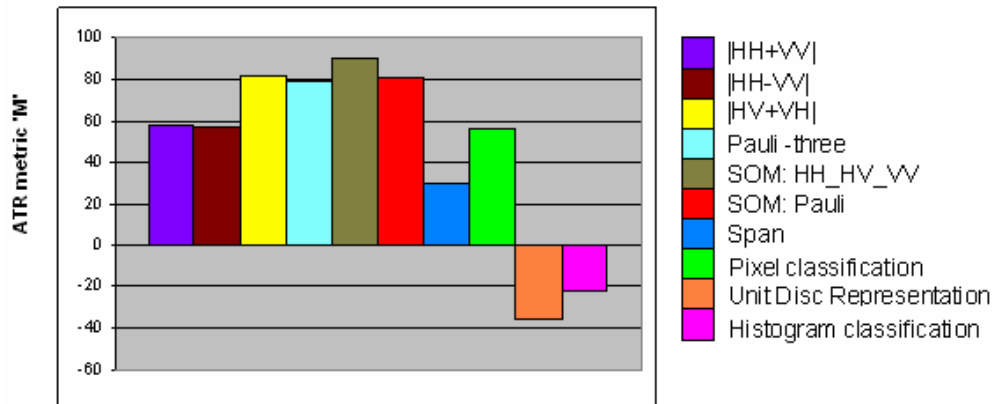
Figure 10. Bar plot of the 'M' ($\overline{P_{cc/d}}$ - P_{fa} .) value for each ATR systems

To compare the full-channels-based ATR system with the single-channel-based ATR system, a single experiment was performed using the single channel |HH| and |VV| features separately, with and without feature enhancement techniques. The classifier (HNeT) and the feature enhancement technique (2DFFT) used in the ATR system are the same as in the full channels based ATR systems. Experimental results are listed in Annex A for more details. Those results are summarized in Table 14 and Table 15. The table 14 shows the summary of average

$\overline{P_{cc/d}}$ for |HH| and |VV| based ATR systems. The ATR systems performs well when the 2DFFT technique is applied on the features. The |VV| based ATR system with 2DFFT technique performed well compared to the performance with the application of other approaches on the single channel dataset. The table 15 shows the summary of average Pfa for |HH| and |VV| based ATR systems. Pfa is minimized when the 2DFFT technique is applied on the |VV| feature. Overall this ATR system performed well as in the full channels based ATR

systems. Therefore, the large positive percentage difference ($\overline{P_{cc/d}}$ – Pfa) in this single channel ATR system is found when both techniques (2DFFT) are applied on the |VV| channel

and the value is 82.62%. Application of this technique resulted in lower $\overline{P_{cc/d}}$ and higher Pfa compared to the full channels SOM (using HH_HV_VV channels) based ATR system.   Most

of the full-channel-based ATR systems performed well in $\overline{P_{cc/d}}$ and single-channel-based ATR system performed well in reducing the false alarm. However, the SOM based HH_VV_VV full channel ATR systems provided the highest correct recognition and low false alarm compared to the other methods.

Table 14. Summary of average $\overline{P_{cc/d}}$ *using single channel based features at $P_d = 90\%$.*

Features	Trained using target & not-A-target samples	
	Normalized	*2DFFT*
|HH|	76.83	92.17
|VV|	77.53	94.44

Table 15. Summary of P_{fa} using single channel based features at $P_d = 90\%$.

Features	Trained using target & not-A-target samples	
	Normalized	*2DFFT*
|HH|	61.82	13.64
|VV|	66.36	11.82

Let's consider the ATR system based on SOM (using HH, HV and VH channels) with the 2DFFT technique, and systems based on |VV| features with 2DFFT technique. ROC curves for both ATR systems are shown in Figure 11. There are 5 curves in both graphs and they are drawn for target A, target B, target D, target G, and all the four targets (target A, B, D and G). All curves in both systems are above the random classifier line. This means, the percentage of correct detection is higher than the percentage of false alarm in any given threshold setting except at the start (maximum threshold rejects all testing objects) and the end (minimum threshold accepts all testing objects) of the curves. The ROC curves for the classifier based on SOM performed slightly better than the classifier based on |VV| at 0.1 percentage of false alarm.
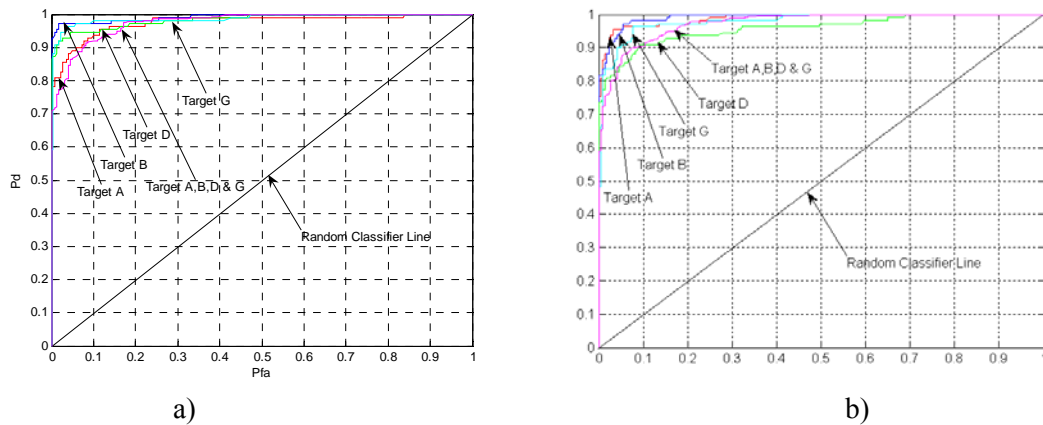
Figure 11. Roc curves for target A, B, D, G and target A B D G using a) ATR system based on SOM and b) ATR system based on |HH|.

The confusion matrices are listed below for these two ATR systems. The confusion matrices for a P_d of 90% are shown below for both of these ATR systems. Table 16 shows the results for the ATR system based on SOM and Table 17 shows the results for the ATR system based on |VV|. Mis-classification and false alarm are less in the SOM based ATR system compared to the other system. A total of 13 confusers are misidentified as target A in the SOM based ATR system and 14 confusers are misidentified as target D in the |VV| based ATR system. The ROC curve for target A in Figure 11a and the ROC curve for target D in Figure 11b are further away from the ideal ROC curve (Ideal ROC curve goes from (0,0) to (1,0) and then from (1,0) to (1,1)) compared to other types of targets.

Table 16. Classifier based on SOM at P_d = 90%.

	A	B	D	G	UNKNOWNS
A	98	0	1	0	11
B	0	98	0	1	11
D	0	0	98	0	12
G	2	0	0	98	10
H	6	0	1	1	102
I	7	0	2	1	100

Table 17. Classifier based on |VV| at P_d = 90%.

	A	B	D	G	UNKNOWNS
A	95	1	0	1	13
B	1	93	2	3	11
D	4	4	94	2	6
G	2	0	2	92	14
H	0	1	12	4	93
I	2	2	2	3	101

8   Conclusions

In this report, a number of ATR systems such as Pauli, SOM, Span, Cameron decomposition and single channel based ATR systems were evaluated. These ATR systems were analyzed based on measures of performance such as, percentage of correct classification over detected targets and percentage of false alarm. Analysis is conducted in many aspects including the effects of selection of training dataset, having of 2DFFT technique, the use of the Cameron method on segmented and non-segmented targets, and a comparison of ATR systems based on full and single channel datasets.

ATR systems trained with training sets including both target and not-a-target samples resulted in fewer false alarms than the systems trained with only target samples. The percentage of correct recognition is almost the same in both systems.   The inclusion of the 2DFFT technique in the ATR system increased the correct recognition rate and reduced the false alarm rate in most of the ATR systems.

Extracted features using the Cameron method are represented in three forms of feature sets; pixel classification, unit disc representation, and histogram classification. These features are extracted from the segmented and non-segmented targets. Overall, the pixel classification based ATR system performed well on the segmented target compared to the other two features (histogram and unit disc representation) and non-segmented targets.

The ATR system based on SOM with HH_HV_VV, including feature enhancement technique of normalization and the 2DFFT performed better in correct recognition and false alarm reduction compared to other single channel or full channel based ATR systems. The average percentage of correct classification achieved is 99% and percentage of false alarm reduced to 8.2% at a percentage of detection of 90%.

Future analysis efforts will perform sensitivity analysis on these methods to provide knowledge regarding the behaviour of these methods under different conditions such as different background, resolution, multi incident angles, etc.

References

[1]   Sources of SAR Data (February 2007). InfoSAR Ltd.
        http://www.infosar.co.uk/docs/node17.html

[2]   Synthetic Aperture Radar Sensors (February 2007). CIESIN Thematic Guides.
        http://www.ciesin.columbia.edu/TG/RS/sarsens.html

[3]   Meth, R. and Chellappa, R. (1996). Automatic classification of targets in Synthetic
        Aperture Radar imagery using topographic features. Algorithms for Synthetic Aperture
        Radar Imagery III. Proceedings of SPIE. Vol. 2757. pp 186 – 193. Orlando, Florida,
        USA.

[4]   Blacknell, D. and Arini, N. S. (2002). Morphological Models for SAR ATR. Algorithms
        for Synthetic Aperture Radar Imagery IX. Proceedings of SPIE. Vol. 4727. pp 69 – 79.
        Orlando, Florida, USA.

[5]   English, R. A., Rawlinson, S. J. and Sandirasegaram, N. M. (2003). ATR workbench for
        automating image analysis. Algorithms for Synthetic Aperture Radar Imagery X.
        Proceedings of SPIE. Vol. 5095. pp 349 – 357. Orlando, Florida, USA.

[6]   Middelmann, W., Ebert, A. and Thoennessen, U. (2005). Kernel-Machine-Based
        Classification in Multi-Polarimetric SAR Data. Algorithms for Synthetic Aperture Radar
        Imagery X. Proceedings of SPIE. Vol. 5808. pp 247 – 256. Orlando, Florida, USA.

[7]   Lee, K.Y., Liew, S.C. and Kwoh, L.K. (2002), Land Cover Classification of NASA/JPL
        Polarimetric Synthetic Aperture Radar (POLSAR) Data over the Tropical Region Using
        Polarimetric Signatures. Proceeding of IEEE International Geoscience and Remote
        Sensing Symposium 2002. vol. 5. pp 2602-2604.

[8]   Honkela, T. (1998). Description of Kohonen's Self-Organizing Map. (Online)
        http://www.cis.hut.fi/~tho/thesis/ (February 2007)

[9]   Starikov, A. (2000). Self-Organizing Maps -- Mathematical Apparatus. (online)
        BaseGroup Labs. http://www.basegroup.ru/neural/som.en.htm (February 2007)

[10]   Cloude, S.R., and Pottier, E. (1996). A Review of Target Decomposition Theorems in
        Radar Polarimetry. IEEE Transactions on Geoscience and Remote Sensing. Vol. 34. No.
        2. pp 498-518.

[11]   Pottier, E. (2003). Polarimetry: From Basics to Applications. IGARSS 2003. Toulouse,
        France.

[12]   Cameron, W.L., Youssef, N.N. and Leung L.K. (1996). Simulated Polarimetric
        Signatures of Primitive Geometrical Shapes. IEEE Transactions on Geoscience and
        Remote Sensing. Vol. 34. No. 3. pp 793-803.

[13]   Touzi, R. and Charbonneau, F. (2002). Characterization of Target Symmetric Scattering Using Polarimetric SARs. IEEE Transactions on geoscience and remote sensing. Vol. 40. No. 11. pp 2507 – 2516.

[14]   MDA (2006). (Online). http://gs.mdacorporation.com/products/sensor/radarsat2/rs2_overview_update.pdf (November 20, 2006).

[15]   Sandirasegaram, N.M. (2002). Automatic Target Recognition in SAR Imagery using a MLP Neural Network. (DRDC Ottawa TM 2002 – 120). Defence R&D Canada - Ottawa.

[16]   Sandirasegaram N.M. (2005). Spot SAR ATR Using Wavelet Features and Neural Network Classifier. (DRDC Ottawa TM 2005-154). Defence R&D Canada – Ottawa.

[17]   Nixon, M.S. and Aguado, A.S. (2002). Feature Extraction and Image Processing, Oxford: Reed Educational and Professional Publishing Ltd.

[18]   Pace, P., Sutherland, J. (2001). "Detection, recognition, identification and tracking of military vehicles using biomimetic intelligence", Automatic Target Recognition XI - SPIE, pp 326-338, Orlando, Florida, USA.

[19]   HNeT2000 Application Development System User's Guide, Artificial Neural Devices Corporation. (2000).

[20]   (online) Artificial Neural Devices Corporation. http://www.andcorporation.com/applications.html (February 18, 2004).

[21]   English, R.A., Rawlinson, S.J. and Sandirasegaram, N.M. (2002). Development of an ATR Workbench. (DRDC Ottawa TM 2002-155), Defence R&D Canada – Ottawa.

[22]   Klepko, R.(1991). The Holographic Neural Network: Performance comparison with other Neural Networks. (DREO TN 91-18), Defence Research Establishment Ottawa.

[23]   Sutherland, J.G. (1990). A Holographic Model of Memory, Learning and Expression, *International Journal of Neural System*, Vol. 1, No.3, pp 259-267.

[24]   Ross, T.D., and Mossing, J.C. (1999). The MSTAR Evaluation Methodology. Algorithms for SAR Imagery VI. pp 705 - 715, Orlando, USA: SPIE

[25]   English, R. A. (2001). Automatic Target Recognition Using HNet. (DREO TM 2001-080), Defence R&D Canada – Ottawa

[26]   Ross, T.D., Velten, V., Mossing, J.C., Worrell, S. and Bryant, M. (1998). Standard SAR ATR Evaluation Experiments using the MSTAR Public Release Data Set. Algorithms for Synthetic Aperture Radar Imagery V, pp 566-573. Orlando, USA: SPIE

Annex A   ATR Results

A.1   Classifiers trained on the target (A, B, D and G) samples

A.1.1   2DFFT Technique

Table A.1. Confusion Matrices; Applied 2DFFT on the extracted features

a) |HH+VV| features

	A	B	D	G	Unknowns
A	84	0	15	5	6
B	5	69	16	10	10
D	14	3	74	10	9
G	6	2	19	64	19
H	52	0	8	10	40
I	60	0	10	7	33

b) |HH-VV| features

	A	B	D	G	Unknowns
A	73	6	17	3	11
B	3	72	27	0	8
D	2	4	82	6	16
G	3	6	27	67	7
H	87	0	5	5	13
I	103	0	0	2	5

c) |HV+VH| features

	A	B	D	G	Unknowns
A	89	1	1	13	6
B	8	81	0	5	16
D	9	5	85	1	10
G	17	0	4	77	12
H	104	0	1	0	5
I	110	0	0	0	0

d) Pauli-three features

	A	B	D	G	Unknowns
A	86	0	6	9	9
B	1	86	5	2	16
D	8	1	92	2	7
G	4	2	6	86	12
H	93	0	3	6	8
I	108	0	0	0	2

E) SOM using HH, HV and VV

	A	B	D	G	Unknowns
A	93	0	1	10	6
B	1	95	2	2	10
D	0	0	95	1	14
G	1	1	1	93	14
H	80	0	4	9	17
I	78	0	3	5	24

f) SOM using the all three Pauli features

	A	B	D	G	Unknowns
A	95	0	1	6	8
B	1	92	3	3	11
D	0	0	95	1	14
G	1	2	0	96	11
H	89	0	2	4	15
I	97	0	2	1	10

g) Span features

	A	B	D	G	Unknowns
A	66	1	20	13	10
B	2	53	32	12	11
D	19	9	62	11	9
G	27	2	24	45	12
H	106	0	2	2	0
I	110	0	0	0	0
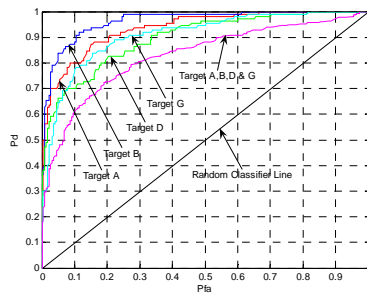
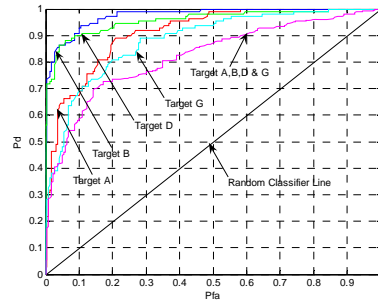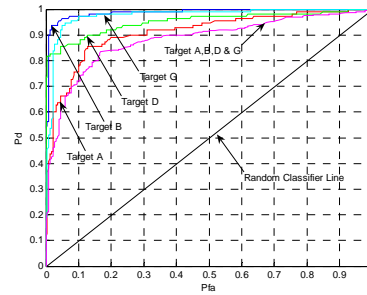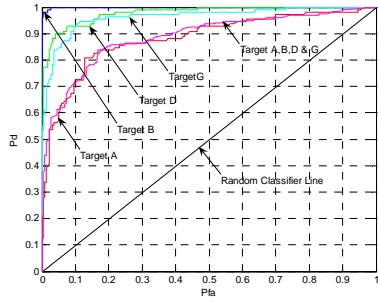a) |HH+VV| features
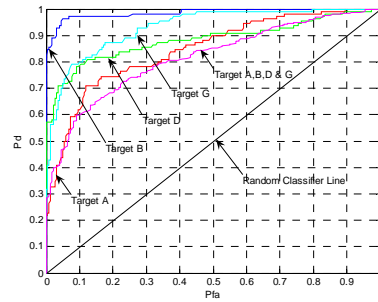
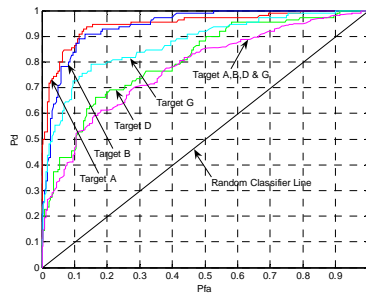b) |HH-VV| features
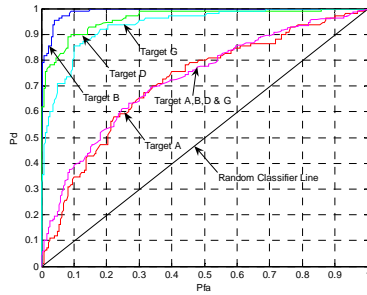
c) |HV+VH| features

d)   Pauli-three features

e) SOM features using HH, HV and VV channels

f) SOM features using the all three Pauli features

g) Span features

Figure A.1. Applied 2DFFT on the extracted features

A.1.2   Normalized and 2DFFT Techniques

Table A.2. Confusion Matrices; Applied normalized and 2DFFT techniques and trained on ABDG

a) |HH+VV| features

	A	B	D	G	Unknowns
A	92	0	5	1	12
B	0	91	3	6	10
D	3	4	89	3	11
G	3	2	5	89	11
H	15	8	18	29	40
I	16	7	33	7	47

b) |HH-VV| features

|	A	B	D	G	Unknowns
A	88	0	3	5	14
B	1	93	2	3	11
D	3	4	92	2	9
G	2	2	3	94	9
H	26	1	38	24	21
I	45	1	16	13	35

c) |HV+VH| features

	A	B	D	G	Unknowns
A	94	1	2	6	7
B	0	92	5	0	13
D	0	5	92	0	13
G	8	0	2	89	11
H	72	1	6	14	17
I	76	3	5	4	22

d) Pauli-three features

	A	B	D	G	Unknowns
A	94	0	0	1	15
B	1	96	0	1	12
D	5	0	97	1	7
G	2	0	1	97	10
H	11	3	11	36	49
I	30	12	5	25	38

E) SOM using HH, HV and VV

	A	B	D	G	Unknowns
A	97	0	0	3	10
B	0	97	0	0	13
D	0	0	97	1	12
G	2	0	1	98	9
H	16	0	15	9	70
I	32	2	9	0	67

f) SOM using the all three Pauli features

	A	B	D	G	Unknowns
A	97	0	0	0	13
B	0	98	0	0	12
D	1	1	97	0	11
G	5	1	0	96	8
H	38	0	6	9	57
I	53	0	1	6	50

g) Span features

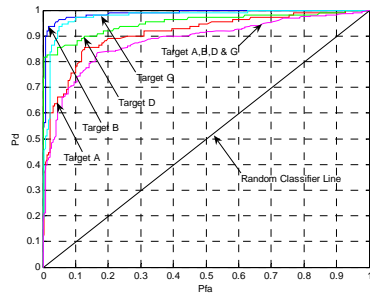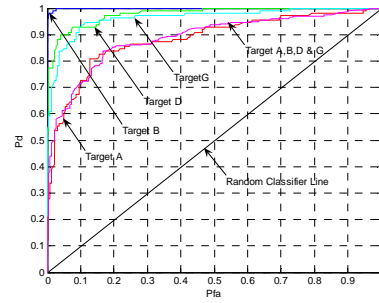|	A	B	D	G	Unknowns
A	92	0	6	5	7
B	0	92	1	3	14
D	8	2	84	4	12
G	2	3	2	92	11
H	5	13	43	31	18
I	12	7	37	31	23
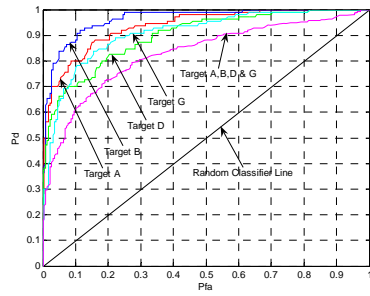
a) |HH+VV| features
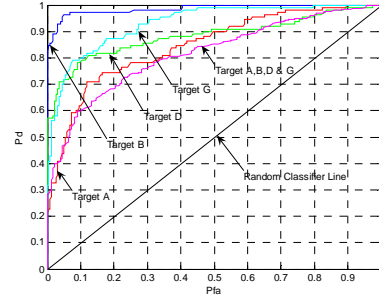
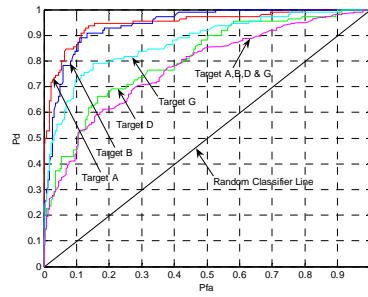b) |HH-VV| features
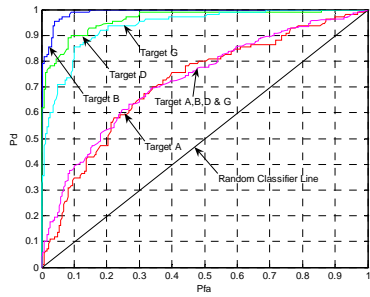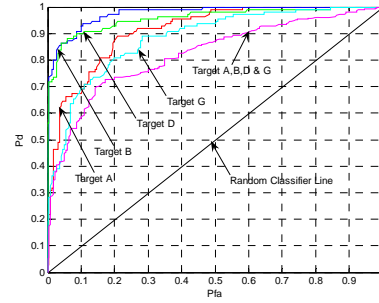
c) |HV+VH| features

d) Pauli-three features

e) SOM features using HH, HV and VV channels

f) SOM features using the all three Pauli features

g) Span features

Figure A.2. Applied normalized and 2DFFT techniques and trained on ABDG

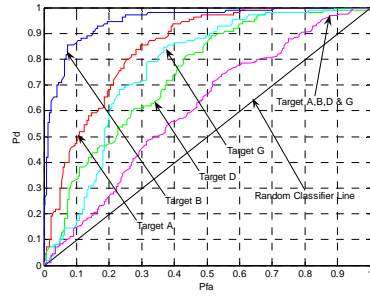## A.2 Classifiers trained on the target and Not-A-Target samples

A.2.1 Normalized technique

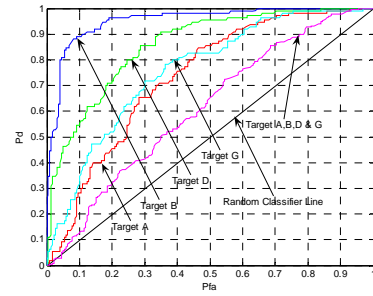*Table A.3. Confusion Matrices; Applied normalized technique and trained on ABDGCEF*

a) |HH+VV| features

	A	B	D	G	Unknowns
A	82	1	7	8	12
B	8	77	8	9	8
D	14	3	73	6	14
G	14	3	10	73	10
H	17	5	31	30	27
I	29	2	29	26	24

b) |HH-VV| features

	A	B	D	G	Unknowns
A	82	0	0	16	12
B	3	81	8	9	9
D	7	5	73	14	11
G	17	3	1	79	10
H	43	2	17	29	19
I	39	4	8	35	24

c) |HV+VH| features

	A	B	D	G	Unknowns
A	76	1	7	13	13
B	7	66	12	7	18
D	5	6	78	12	9
G	25	5	5	71	4
H	36	0	15	27	32
I	34	2	13	34	27

d) Pauli-three features

	A	B	D	G	Unknowns
A	81	0	3	10	16
B	2	87	6	5	10
D	8	1	87	1	13
G	13	1	3	88	5
H	26	2	14	31	37
I	34	5	13	21	37

E) SOM using HH, HV and VV

	A	B	D	G	Unknowns
A	68	7	4	17	14
B	15	59	14	9	13
D	23	0	71	8	8
G	23	2	10	66	9
H	25	6	15	11	53
I	21	8	12	6	63

f) SOM using the all three Pauli features

	A	B	D	G	Unknowns
A	78	0	1	18	13
B	6	83	6	3	12
D	10	3	72	12	13
G	24	4	3	73	6
H	29	2	13	29	37
I	49	0	12	10	39

g) Span features

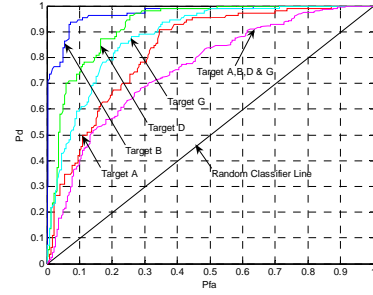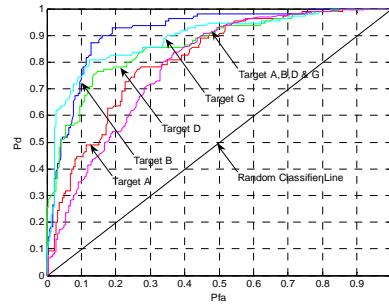|	A	B	D	G	Unknowns
A	86	2	3	11	8
B	0	84	5	7	14
D	11	1	82	5	11
G	14	3	3	80	10
H	11	8	39	37	15
I	13	12	40	23	22

a) |HH+VV| features

b) |HH-VV| features
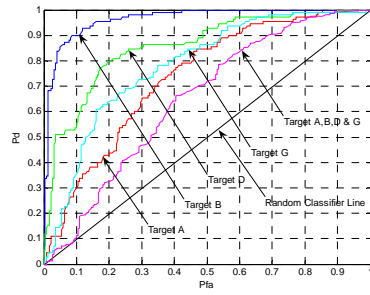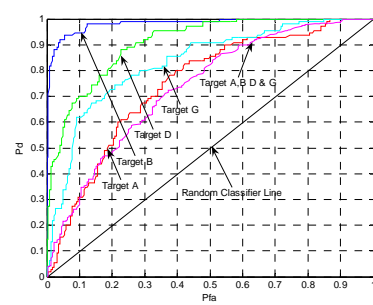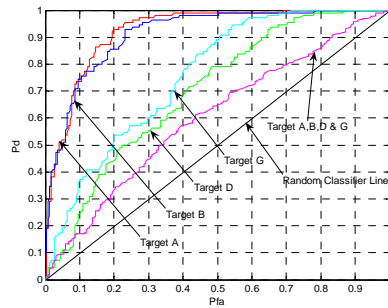
c) |HV+VH| features

d) Pauli-three features

e) SOM features using HH, HV and VV

f) SOM features using the all three Pauli features

g) Span features
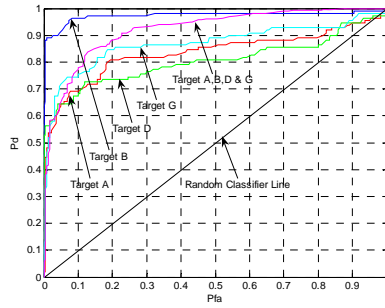
Figure A.3. Applied normalized technique

A.2.2   2DFFT Technique

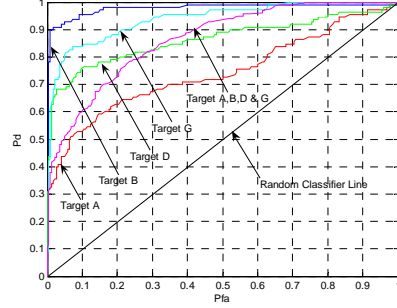*Table A.4. Confusion Matrices; Applied 2DFFT technique and trained on ABDGCEF*

a) |HH+VV| features

	A	B	D	G	Unknowns
A	76	0	20	7	7
B	10	46	38	7	9
D	18	9	70	6	7
G	11	1	23	55	20
H	16	0	14	4	76
I	23	0	9	1	77

b) |HH-VV| features

	A	B	D	G	Unknowns
A	68	2	28	1	11
B	11	59	25	0	15
D	18	6	75	4	7
G	5	4	23	67	11
H	38	0	9	4	59
I	51	0	6	0	53

c) |HV+VH| features

	A	B	D	G	Unknowns
A	78	1	6	16	9
B	4	77	6	2	21
D	5	7	85	4	9
G	15	1	2	87	5
H	33	0	3	1	73
I	29	0	0	1	80

d) Pauli-three features

	A	B	D	G	Unknowns
A	94	0	3	2	11
B	1	91	6	1	11
D	9	2	89	1	9
G	3	2	4	88	13
H	24	0	4	1	81
I	20	0	1	0	89

E) SOM using HH, HV and VV

	A	B	D	G	Unknowns
A	91	0	3	6	10
B	2	90	2	2	14
D	4	1	93	0	12
G	5	2	3	92	8
H	33	0	4	6	67
I	23	0	3	2	82

f) SOM using the all three Pauli features

	A	B	D	G	Unknowns
A	93	0	3	2	12
B	2	93	3	0	12
D	2	1	96	2	9
G	6	1	2	90	11
H	30	0	1	2	77
I	22	0	1	1	86

g) Span features

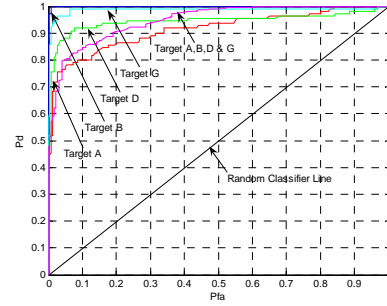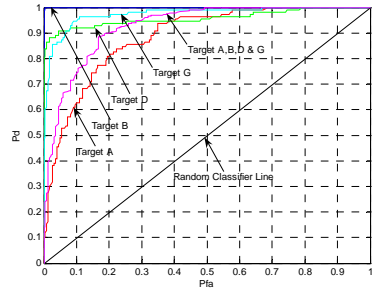|	A	B	D	G	Unknowns
A	51	0	45	4	10
B	4	45	40	12	9
D	22	7	67	9	5
G	13	0	38	39	20
H	0	0	101	1	8
I	0	0	103	0	7

a) |HH+VV| features

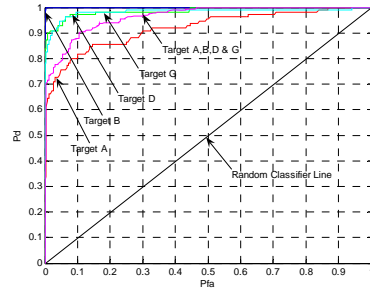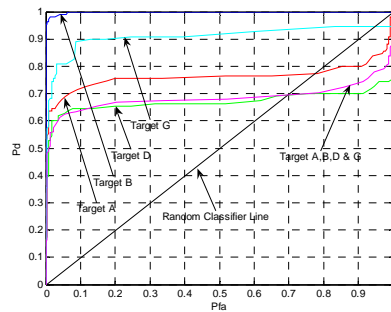b) |HH-VV| features
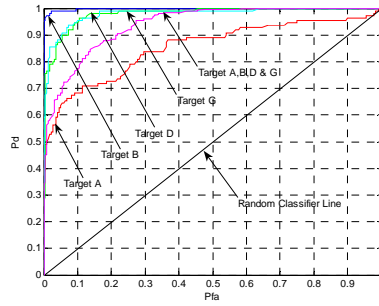
c) |HV+VH| features

d) Pauli-three features

e) SOM features using HH, HV and VV

f) SOM features using the all three Pauli features

g) Span features
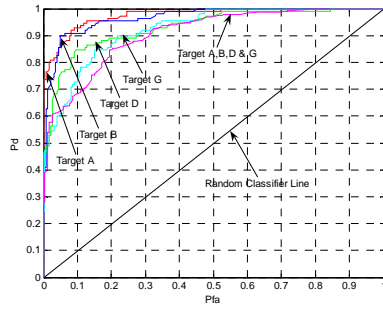
Figure A.4. Applied 2DFFT technique and trained on ABDGCEF

A.2.3   Normalized and 2DFFT Techniques

*Table A.5. Confusion Matrices; Applied normalized and 2DFFT techniques and trained on ABDGCEF*

a) |HH+VV| features

	A	B	D	G	Unknowns
A	91	0	6	2	11
B	0	93	3	4	10
D	2	2	94	3	9
G	2	1	5	88	14
H	3	2	20	19	66
I	4	8	10	11	77

b) |HH-VV| features

	A	B	D	G	Unknowns
A	91	1	4	1	13
B	1	92	4	1	12
D	0	4	95	2	9
G	2	1	5	92	10
H	6	0	29	14	61
I	16	1	9	5	79

c) |HV+VH| features

	A	B	D	G	Unknowns
A	95	0	0	4	11
B	0	96	2	1	11
D	1	3	93	1	12
G	7	0	0	93	10
H	9	0	1	9	91
I	9	0	0	1	100

d) Pauli-three features

	A	B	D	G	Unknowns
A	96	0	1	1	12
B	0	96	2	3	9
D	2	2	93	0	13
G	3	1	1	95	10
H	0	0	10	8	92
I	4	0	8	8	90

E) SOM using HH, HV and VV

	A	B	D	G	Unknowns
A	98	0	1	0	11
B	0	98	0	1	11
D	0	0	98	0	12
G	2	0	0	98	10
H	6	0	1	1	102
I	7	0	2	1	100

f) SOM using the all three Pauli features

	A	B	D	G	Unknowns
A	96	0	0	2	12
B	0	98	1	3	8
D	0	0	97	0	13
G	2	0	0	97	11
H	4	0	10	7	89
I	5	0	3	9	93

g) Span features

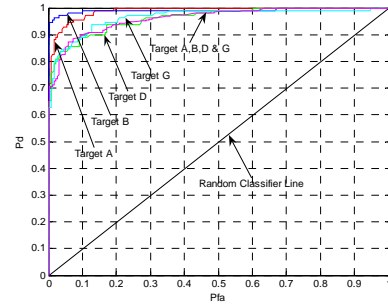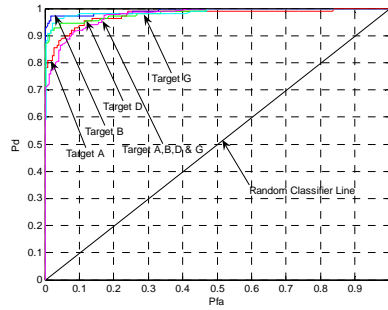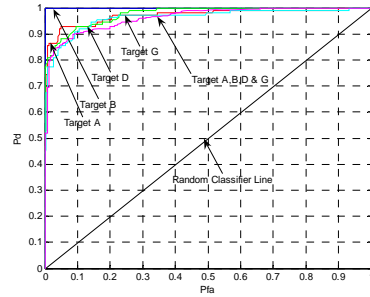|	A	B	D	G	Unknowns
A	94	0	4	5	7
B	0	94	0	2	14
D	6	3	89	2	10
G	8	1	3	85	13
H	2	7	33	39	29
I	6	10	22	23	49

a) |HH+VV| features
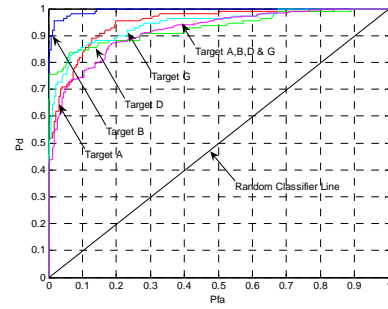
b) |HH-VV| features
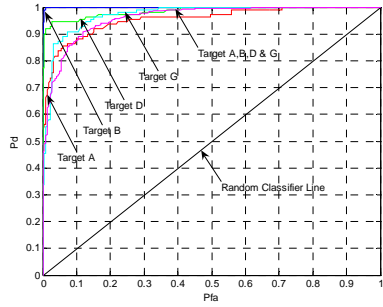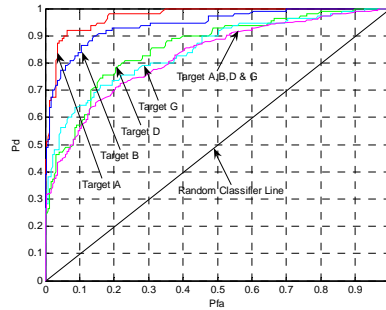

c) |HV+VH| features

d) Pauli-three features

e) SOM features using HH, HV and VV

f) SOM features using the all three Pauli features

g) Span features

Figure A.5. Applied normalized and 2DFFT techniques and trained on ABDGCEF

A.3 Cameron decomposition based Classifiers trained on the target and Not-A-Target samples

A.3.1 Cameron decomposition based ATR applied on non-segmented target

Table A.6. Confusion Matrices; Cameron decomposition based ATR on non-segmented targets and trained on ABDGCEF

<table>
<tr><td colspan="6">a) Pixel classification</td><td colspan="6">b) Unit Disc Representation</td></tr>
<tr><td></td><td>A</td><td>B</td><td>D</td><td>G</td><td>Unknowns</td><td></td><td>A</td><td>B</td><td>D</td><td>G</td><td>Unknowns</td></tr>
<tr><td>A</td><td>55</td><td>10</td><td>14</td><td>20</td><td>9</td><td>A</td><td>48</td><td>20</td><td>20</td><td>9</td><td>11</td></tr>
<tr><td>B</td><td>36</td><td>24</td><td>13</td><td>22</td><td>13</td><td>B</td><td>38</td><td>14</td><td>34</td><td>14</td><td>8</td></tr>
<tr><td>D</td><td>39</td><td>14</td><td>19</td><td>20</td><td>16</td><td>D</td><td>37</td><td>16</td><td>28</td><td>15</td><td>12</td></tr>
<tr><td>G</td><td>47</td><td>17</td><td>11</td><td>28</td><td>5</td><td>G</td><td>38</td><td>14</td><td>32</td><td>13</td><td>11</td></tr>
<tr><td>H</td><td>51</td><td>8</td><td>14</td><td>14</td><td>21</td><td>H</td><td>42</td><td>16</td><td>20</td><td>15</td><td>15</td></tr>
<tr><td>I</td><td>50</td><td>15</td><td>8</td><td>21</td><td>14</td><td>I</td><td>45</td><td>16</td><td>19</td><td>13</td><td>15</td></tr>
</table>

<table>
<tr><td colspan="6">c) Histogram classification</td></tr>
<tr><td></td><td>A</td><td>B</td><td>D</td><td>G</td><td>Unknowns</td></tr>
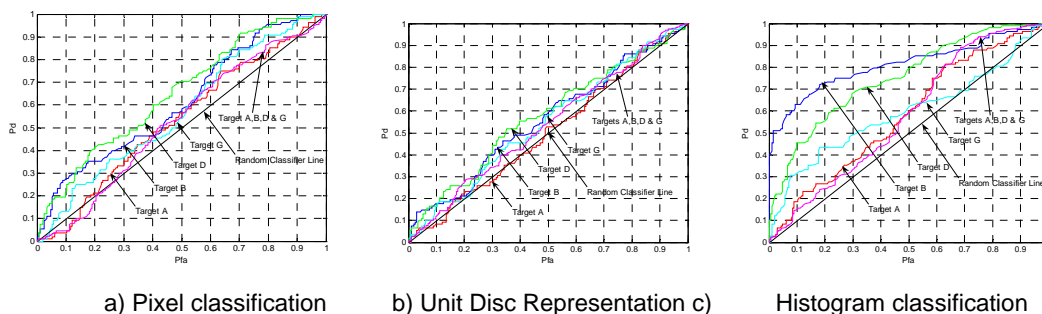<tr><td>A</td><td>71</td><td>4</td><td>10</td><td>7</td><td>16</td></tr>
<tr><td>B</td><td>36</td><td>48</td><td>12</td><td>5</td><td>7</td></tr>
<tr><td>D</td><td>47</td><td>5</td><td>29</td><td>20</td><td>7</td></tr>
<tr><td>G</td><td>55</td><td>5</td><td>17</td><td>18</td><td>13</td></tr>
<tr><td>H</td><td>64</td><td>6</td><td>5</td><td>4</td><td>29</td></tr>
<tr><td>I</td><td>57</td><td>3</td><td>8</td><td>5</td><td>35</td></tr>
</table>

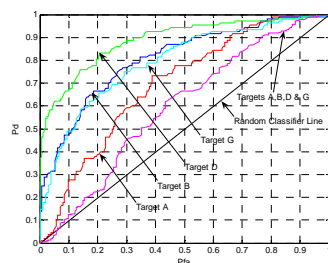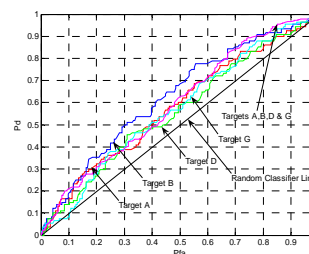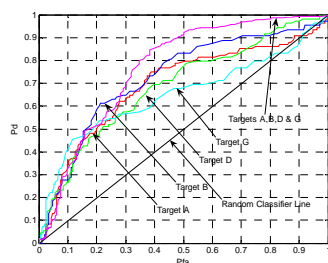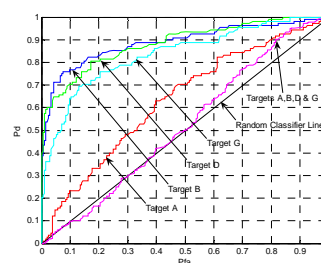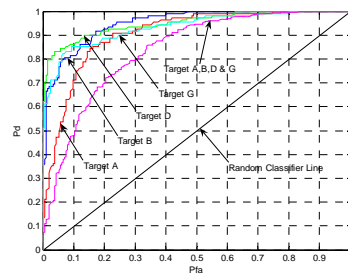a) Pixel classification   b) Unit Disc Representation c)   Histogram classification

Figure A.6. ROC curves; Cameron decomposition based ATR on non-segmented targets and trained on ABDGCEF

A.3.2   Cameron decomposition and 2DFFT based ATR applied on non-segmented data and trained on ABDGCEF samples
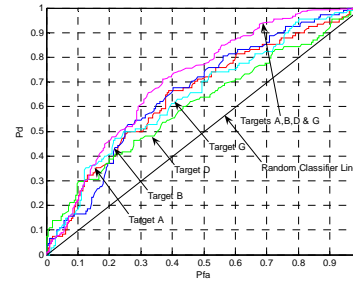
Table A.7.   Confusion Matrices; Cameron decomposition and 2DFFT based ATR on non-segmented data

a) Pixel classification

	A	B	D	G	Unknowns
A	69	6	3	21	9
B	16	40	9	33	10
D	23	22	34	15	14
G	27	28	16	29	8
H	42	10	17	17	22
I	55	6	8	12	27

b) Unit Disc Representation

	A	B	D	G	Unknowns
A	58	2	17	11	20
B	35	26	20	20	7
D	43	11	33	16	5
G	40	11	19	29	9
H	57	4	13	23	11
I	54	2	11	26	15

c) Histogram classification

	A	B	D	G	Unknowns
A	91	0	5	0	12
B	103	1	1	0	3
D	92	2	0	4	10
G	97	0	0	0	11
H	91	0	3	1	13
I	101	0	1	0	6
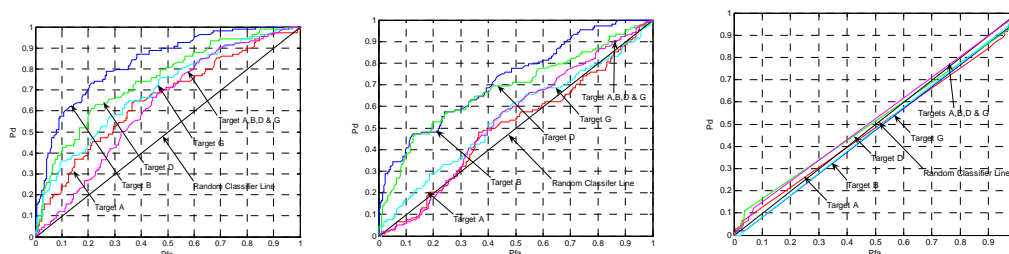
a) Pixel classification   b) Unit Disc Representation   c) Histogram classification

Figure A.7.   ROC curves for Cameron method; Cameron decomposition and 2DFFT based ATR on non-segmented data

A.3.3 Cameron decomposition based ATR applied on segmented data and trained on ABDGCEF samples

Table A.8. Cameron decomposition based ATR on segmented targets

a) Pixel classification

	A	B	D	G	Unknowns
A	81	4	0	9	14
B	33	59	5	8	3
D	22	9	61	5	11
G	28	14	1	51	14
H	53	14	7	11	23
I	43	19	3	11	32

b) Unit Disc Representation

	A	B	D	G	Unknowns
A	54	12	12	17	13
B	50	17	12	21	8
D	50	12	12	22	12
G	61	14	10	13	10
H	52	13	7	14	22
I	44	3	16	15	30

c) Histogram classification

	A	B	D	G	Unknowns
A	76	2	10	2	18
B	82	7	14	0	5
D	76	4	15	2	11
G	80	8	11	0	9
H	49	2	9	2	46
I	33	4	2	1	68

d) Pixel classification: Rotated to common orientation

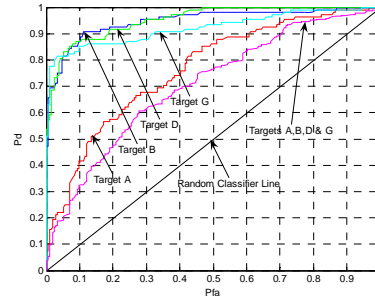|	A	B	D	G	Unknowns
A	83	1	9	7	8
B	14	67	5	11	11
D	16	14	63	2	13
G	15	8	9	66	10
H	52	6	4	14	32
I	74	2	2	12	18

a) Pixel classification

b) Unit Disc Representation

c) Histogram classification

d) Pixel classification; rotated to common orientation

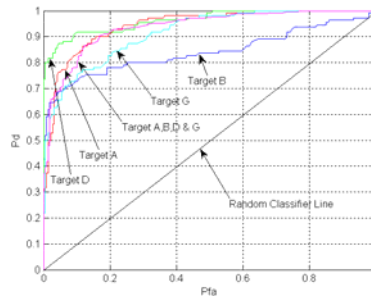## A.3.4 Cameron decomposition and 2DFFT based ATR applied on segmented data and trained on ABDGCEF samples

Table A.9. Cameron method and 2DFFT techniques applied on segmented data

a) Pixel classification					**b)** Unit Disc Representation				
	A	**B**	**D**	**G**	**Unknowns**	**A**	**B**	**D**	**G**	**Unknowns**
A	84	1	5	7	11	58	7	22	11	10
B	4	81	2	10	11	56	11	15	18	8
D	8	3	83	6	8	41	10	26	15	16
G	4	4	2	85	13	52	18	16	13	9
H	14	8	4	6	76	43	9	8	8	40
I	18	4	4	6	76	37	9	12	11	39

c) Histogram classification					d) Pixel classification: Rotated to common orientation				
	A	**B**	**D**	**G**	**Unknowns**	**A**	**B**	**D**	**G**	**Unknowns**
A	96	0	0	0	12	89	0	1	10	8
B	97	0	0	0	11	1	77	2	15	13
D	101	0	0	0	7	4	1	88	5	10
G	95	0	0	0	13	2	2	9	84	11
H	96	0	0	0	12	44	6	8	5	45
I	94	0	0	0	14	66	2	3	5	32

a) Pixel classification

b) Unit Disc Representation

c) Histogram classification

d) Pixel classification; rotated to common orientation

A.4   Single Channel (HH and VV) based ATR

Table A.10. Single Channel based ATR and Train on ABDGCEF

a) **|HH| features**	A	B	D	G	Unknowns
A	81	0	2	13	14
B	3	67	20	13	7
D	4	7	77	13	9
G	5	8	12	71	14
H	3	2	10	20	75
I	4	2	6	14	84

b) **| VV| features**	A	B	D	G	Unknowns
A	67	11	1	14	17
B	6	78	10	14	2
D	4	26	70	1	9
G	6	26	2	61	15
H	7	27	1	5	70
I	0	15	0	5	90

c) **Normalization applied on |HH|**	A	B	D	G	Unknowns
A	75	2	2	17	14
B	6	76	10	11	7
D	4	7	79	9	11
G	6	3	15	75	11
H	10	4	16	37	43
I	19	1	27	22	41

d) **Normalization applied on |VV|**	A	B	D	G	Unknowns
A	85	1	1	17	6
B	5	78	12	7	8
D	2	13	76	6	13
G	15	5	5	68	17
H	11	12	15	32	40
I	27	9	25	15	34

E) **2DFFT applied on |HH|**	A	B	D	G	Unknowns
A	71	2	9	12	16
B	7	68	22	12	1
D	6	3	81	11	9
G	4	2	23	64	17
H	0	0	12	1	97
I	0	0	6	0	104

f) **2DFFT applied on |VV|**	A	B	D	G	Unknowns
A	76	0	18	5	11
B	12	47	24	16	11
D	12	1	81	7	9
G	13	3	20	62	12
H	4	0	14	2	90
I	6	0	7	3	94

g) **Normalization and 2DFFT applied on |HH|**	A	B	D	G	Unknowns
A	93	0	1	9	7
B	4	97	0	1	8
D	4	2	87	3	14
G	3	0	4	88	15
H	2	0	10	3	95
I	1	0	14	0	95

h) **Normalization and 2DFFT applied on |VV|**	A	B	D	G	Unknowns
A	95	1	0	1	13
B	1	93	2	3	11
D	4	4	94	2	6
G	2	0	2	92	14
H	0	1	12	4	93
I	2	2	2	3	101

a) |HH| features

b) |VV| features
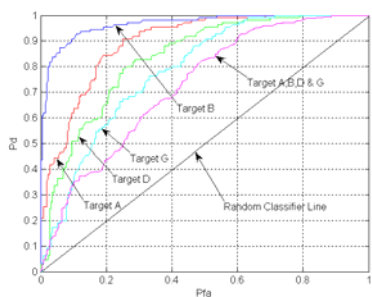
c) Normalization applied on |HH|
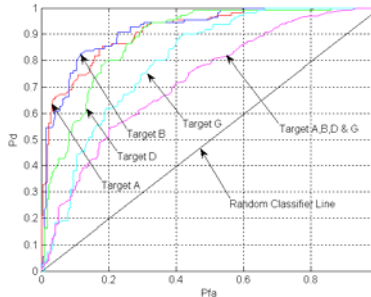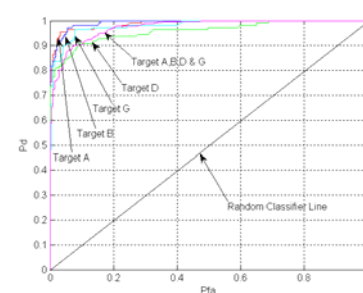
d) Normalization applied on |VV|
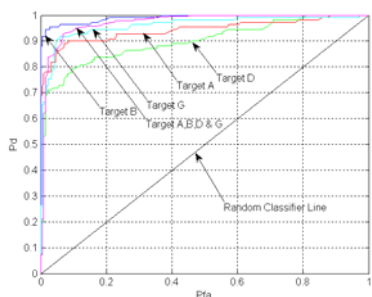
e) 2DFFT applied on |HH|
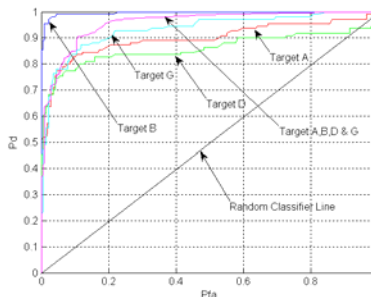
f) 2DFFT applied on |VV|
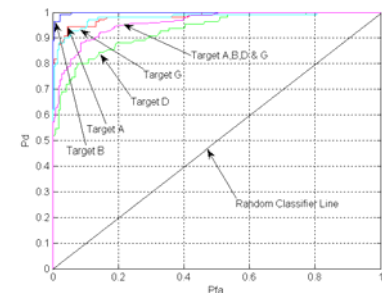
g) Normalization and 2DFFT applied on |HH|

h) Normalization and 2DFFT applied on |VV|

Figure A.10. ROC curves for Single Channel; Trained on ABDGCEF

List of symbols/abbreviations/acronyms/initialisms

2DFFT	Two-Dimensional Fast Fourier Transform
ATR	Automatic Target Recognition
DRDC	Defence Research & Development Canada
FFT	Fast Fourier Transform
HNeT	Holographic Neural Technology
HH	Horizontal transmit and Horizontal receive
HV	Horizontal transmit and Vertical receive
NATO	North Atlantic Treaty Organization
Pcc/d	Percentage of Correct Classification over detected targets
Pd	Percentage of target detection
Pfa	Percentage of false alarm
ROC	Receiver Operating Characteristic
SOM	Self-Organizing-Map
SET	Sensors & Electronics Technology
SAR	Synthetic Aperture Radar
VH	Vertical transmit and Horizontal receive
VV	Vertical transmit and Vertical receive

Distribution list

Document No.: DRDC Ottawa TM 2007-330

LIST PART 1: Internal Distribution by Centre

2	Author
2	DRDC Library
1	Head / Radar Application and Space Technologies
1	Leader / Radar Data Exploitation – Targets / RAST
1	Leader / Radar Data Exploitation – Signatures / RAST
1	Leader / Surveillance Radar / RS

8	TOTAL LIST PART 1

LIST PART 2: External Distribution by DRDKIM

3	Library and Archives Canada (2 HC, 1 CD)
1	DRDC ATLANTIC / Head / Signatures
1	ADM(S&T) (for distribution)
1	DRDKIM 3 (CD)
1	DSTC4ISR 5 (Attn: Caroline Wilcox)
1	CDI D Geo Int (Attn: Maj John Klatt)
1	DJCP (Attn: LCdr Andy Samoluk)
1	DGIMPD DPDOIS (Attn: LCol Jeff Howes)
1	DJCP (Attn: LCdr R. Quinn)
1	MCE (Attn: Pierre Simard)
1	CFJIC (Attn: Maj. Bourget)
1	CF School of Aerospace Studies
1	PMO Aurora (Library)

15	TOTAL LIST PART 2

23 TOTAL COPIES REQUIRED

13. ABSTRACT (A brief and factual summary of the document. It may also appear elsewhere in the body of the document itself. It is highly desirable that the abstract of classified documents be unclassified. Each paragraph of the abstract shall begin with an indication of the security classification of the information in the paragraph (unless the document itself is unclassified) represented as (S), (C), (R), or (U). It is not necessary to include here abstracts in both official languages unless the text is bilingual.)

Reduction of false alarm with acceptable accuracy of classification rate is a challenge in Automatic Target Recognition (ATR) using Synthetic Aperture Radar (SAR) images. This report addresses the evaluation of polarimetric techniques features, benefits of applying Two-Dimensional Fourier Transform on the polarimetric features, and the technique of training data selection to improve the classification accuracy and to reduce the false alarm in small stationary targets of high-resolution full polarimetric SAR images. The Pauli and Cameron decompositions, Self Organizing Maps, and Span techniques are applied on the polarimetric data and then Two-Dimensional Fourier Transform is applied to improve the performance. Two types of training data (one with samples of target only and the other with samples of target and Not-a-target) are used to train the Holographic Neural Technology (a neural network) classifier. The results show the Self Organizing Map feature extraction technique with Fourier Transform algorithm has a better classification rate and low false alarm. The ATR system trained with samples of target and not-a-target, produced low false alarm compared to the one trained with samples of target alone.

14. KEYWORDS, DESCRIPTORS or IDENTIFIERS (Technically meaningful terms or short phrases that characterize a document and could be helpful in cataloguing the document. They should be selected so that no security classification is required. Identifiers, such as equipment model designation, trade name, military project code name, geographic location may also be included. If possible keywords should be selected from a published thesaurus, e.g. Thesaurus of Engineering and Scientific Terms (TEST) and that thesaurus identified. If it is not possible to select indexing terms which are Unclassified, the classification of each should be indicated as with the title.)

ATR,Automatic Target Recognition, HNeT,Holographic Neural Technology, ROC, Receiver Operating Characteristic,2DFFT, Two-Dimensional Fast Fourier Transform,Confusion Matrix, Cameron, Pauli, SOM, Self Organizing Map